

1 **Contrasted trends in phytoplankton diversity, size structure and carbon burial efficiency**
2 **in the Mediterranean Sea under shifting environmental conditions**

3 **Camille Godbillot¹, Baptiste Pesenti¹, Karine Leblanc², Luc Beaufort¹, Cristele Chevalier², Julien**
4 **Di Pane^{2,*}, Xavier Durrieu de Madron³, Thibault de Garidel-Thoron¹**

5 ¹Aix-Marseille Univ, CNRS, IRD, INRAE, CEREGE, ITEM – Aix-en-Provence, France

6 ²Aix-Marseille Univ, Université de Toulon, CNRS, IRD, MIO UM110 – Marseille, France

7 ³CEFREM, CNRS, Université de Perpignan Via Domitia – Perpignan, France

8

9 Corresponding author: Camille Godbillot (godbillot@cerege.fr)

10 *Now at: EDF R&D, LNHE - Laboratoire National d'Hydraulique et Environnement – Chatou,
11 France

12 **Key Points:**

- 13 • Carbon burial pathways differ across NW Mediterranean Sea sites, in particular due to
14 deep convection dynamics.
- 15 • Between 2010 and 2019, biological particle and organic matter fluxes to the seafloor
16 declined, mirroring a decrease in vertical mixing.
- 17 • Contrary to the Gulf of Lion, calcareous phytoplankton is becoming dominant in the
18 Ligurian Sea, decreasing carbon burial efficiency.
- 19

20 **Abstract**

21 Shifts in the phytoplankton assemblage induced by environmental changes have significant
22 implications for carbon cycling and marine food webs, but remain poorly constrained across
23 spatiotemporal scales. Here, we investigate the effects of rising sea surface temperatures and
24 increased stratification on the phytoplankton composition and size in Northwestern
25 Mediterranean Sea (2010-2019) using two sediment trap series: one in the oligotrophic Ligurian
26 Sea and the other in the deep convection zone of the Gulf of Lion. We apply deep-learning
27 image analysis to quantify phytoplankton particle fluxes, size distributions, and relative
28 assemblages, focusing on coccolithophores, diatoms, and silicoflagellates. Our results show a
29 general decline of phytoplankton fluxes to the seafloor, mirroring the decrease in vertical
30 mixing in the water column. Both sites show a shift towards phytoplankton species adapted to
31 stratified and nutrient-depleted conditions, although with contrasting patterns. In the Ligurian
32 Sea, deep-dwelling coccolithophore species become dominant, while in the Gulf of Lion,
33 summer-associated siliceous species, including large diatoms and silicoflagellates, show an
34 increase. These contrasted trends, which likely result from differences in nutrient inputs and pH
35 changes in the surface between the two sites, have implications for the efficiency of carbon
36 export pathways at depth. Specifically, the increasing dominance of smaller phytoplankton in
37 the Ligurian Sea leads to a reduction in carbon burial efficiency, while in the Gulf of Lion, the
38 enhanced contribution of larger diatoms may sustain relatively higher export and burial rates in
39 the future.

40

41 **Plain Language Summary**

42 Phytoplankton are small marine plants that make up the base of the food web. They play a key
43 role in regulating Earth's climate by removing carbon dioxide from the sea surface and
44 transporting it to the deep ocean, preventing it from interacting with the atmosphere. Ongoing
45 climate change is altering the species composition and size of phytoplankton, with potential
46 effects on carbon cycling. Here, we investigated the effects of rising temperatures and ocean
47 mixing on the phytoplankton community at two sites from the Northwestern Mediterranean
48 Sea between 2010 and 2019. Using artificial intelligence to study microscope images, we found
49 that fewer phytoplankton remains were sinking to the seafloor, an observation that could be
50 attributed, in part, to the increasing temperatures affecting phytoplankton growth in the
51 surface, and in part to their slower transport at depth under decreasing mixing conditions.
52 However, in the Gulf of Lion, an area affected by faster acidification, diatom species are
53 becoming dominant. Due to their large size, this offsets, in part, the decrease in carbon fluxes
54 to the seafloor. As the Mediterranean continues to warm, the observed trends could weaken its
55 role as a carbon sink, affecting regional carbon cycling and marine ecosystems.

56

57 1 Introduction

58 Human-induced greenhouse warming increases water column stratification (Li et al., 2020),
59 which in turn reduces nutrient availability in surface waters. Larger phytoplankton cells, due to
60 their smaller surface-to-volume ratio, are more prone to nutrient limitation compared to
61 smaller cells, and thus tend to decline in nutrient-depleted surface waters (Falkowski & Oliver,
62 2007). A number of studies has pointed out an increase in the proportion of small-sized species
63 in the phytoplankton assemblage together with warming conditions, whether on short
64 timescales (Iriarte & González, 2004) or longer, decadal timescales (Beaugrand, 2004; Di Pane
65 et al., 2022; Suikkanen et al., 2013). These shifts occur among species within a single group, or
66 occur over different phytoplankton groups. In turn, changes in the size and taxonomic
67 composition of phytoplankton have significant implications for food web dynamics and marine
68 biogeochemistry (Finkel et al., 2010). For example, an increasing dominance of smaller
69 phytoplankton in the surface has been linked to the emergence of microbial loops and a
70 reduction in carbon export from the surface (Iriarte & González, 2004). This is because large
71 phytoplankton sink more rapidly, and because they are more likely to aggregate into large
72 particles that are exported quickly from the surface (Thornton, 2002). In the sea, the main
73 eukaryotic phytoplankton groups are diatoms, coccolithophores, and dinoflagellates. *In situ* and
74 modelling studies confirm that diatoms, a group of silicifying phytoplankton, are more efficient
75 for carbon export from the surface than coccolithophores, their calcifying – and relatively
76 smaller – counterparts (Jin et al., 2006; Mayot et al., 2017).

77 The Mediterranean Sea stands out as a hotspot of ongoing environmental changes, making it a
78 key region for investigating shifts in the structure of planktonic communities. Despite a densely
79 populated coast relying on its production, the Mediterranean Sea is a predominantly
80 oligotrophic region, characterized by low nutrient levels and chlorophyll concentrations. The
81 Northwestern part of the Mediterranean stands out as a more productive area (D’Ortenzio,
82 2009) due to Atlantic influx, riverine discharge, atmospheric deposition and deep ocean
83 convection (Severin et al., 2014). This last process is important for replenishing the surface in
84 nutrients, and for storing carbon in the deep sea (Conan et al., 2018; Gogou et al., 2014; Macias
85 et al., 2018; Touratier et al., 2016). Studies have documented that these events, caused by cold
86 and windy winters, trigger spring blooms of higher intensity than average (Mayot et al., 2017).
87 Recent decades have seen changes in Mediterranean ocean processes, and accompanying
88 changes in phytoplankton productivity. The Mediterranean Sea has been warming since the
89 1960s (Bethoux & Gentili, 1999), with summer temperatures increasing 40% faster than the
90 global mean (Cramer et al., 2018; Lionello & Scarascia, 2018). In parallel, deep convection
91 episodes under the worst-case climate change scenarios are likely to collapse by the mid-21st
92 century due to the strengthening of vertical stratification itself caused by the warming of
93 surface and intermediate waters (Parras-Berrocal et al., 2022; Somot et al., 2006). Margirier et
94 al. (2020) already documented a marked reduction in deep convection events between 2010
95 and 2018, in conjunction with significant warming and salinization during this period.

96 The recent increase in Mediterranean Sea surface temperatures, and the associated increase in
97 water column stratification, have an impact on the phytoplankton community. Between 1991
98 and 1997, a study on the DYFAMED sampling site in the Ligurian Sea suggested that the
99 lengthening of the stratification period led to the increasing domination of smaller

100 phytoplankton in the surface relative to diatoms (Marty et al., 2002). More recently, a study
101 from a coastal site near Marseille reported an increase in the proportion of diatoms relative to
102 dinoflagellates as well as a decrease in pico- and nanophytoplankton size between 2005 and
103 2020 (Garcia et al., 2023). The authors attribute these changes to the shifting environmental
104 conditions, in particular a relative increase in nitrate concentrations relative to phosphate and
105 nitrite levels (Garcia et al., 2023). The implications of these community changes for
106 biogeochemical cycling—a critical question for understanding the impacts of climate change—
107 remain poorly constrained. For instance, the increase in smaller phytoplankton was associated
108 with increased biomass in the study by Marty et al. (2002). Additionally, the contribution of
109 different phytoplankton groups – and species – to carbon burial remains uncertain due to their
110 varying efficiency in being exported from surface waters (Leblanc et al., 2018; Williams et al.,
111 2024). Disentangling the effects of shifts in species composition and cell size on carbon export
112 and burial therefore represents a significant scientific challenge.

113 The northwestern Mediterranean Sea (NW Mediterranean Sea) has benefited from extensive
114 observation projects on particle fluxes, including the use of sediment traps (Gogou et al., 2014;
115 Miquel et al., 2011; Stabholz et al., 2013). Despite intrinsic limitations (Buesseler et al., 2007),
116 sediment traps remain the most efficient way to resolve both the spatial and temporal
117 (seasonal, yearly) diversity of the phytoplankton assemblage that reaches the deeper layers of
118 the sea. When positioned near the seafloor, they yield information on phytoplankton
119 production in the surface waters, as well as on the biological cycling and export efficiency at the
120 site. In this study, we investigate two sediment trap series from the NW Mediterranean Sea
121 spanning the period between 2010 and 2019: one located in the Ligurian Sea located in the
122 oligotrophic Ligurian current, and the other off the Gulf of Lion’s plateau within the deep
123 convection zone. We use deep-learning based approaches to detect, classify, and measure the
124 microorganisms we observe in the microscope images we obtain from the sediment trap
125 samples (Beaufort & Dollfus, 2004; Godbillot et al., 2024). Trends in phytoplankton community
126 composition and size structure are compared to the environmental records for the sites, as well
127 as the carbon fluxes to the trap, to improve our understanding of the linkages between
128 environmental changes, biological community dynamics, and their implications for
129 biogeochemical cycling in a rapidly changing Mediterranean ecosystem.

130 **2 Materials and Methods**

131 **2.1 Site locations and material preservation**

132 Here we investigate two time series from the NW Mediterranean Sea, from the Gulf of Lion and
133 from the Ligurian Sea (**Figure 1**). The sediment trap series are respectively referred to as the
134 Lionceau and DYFAMED moorings in this text.

135 The Lionceau mooring (42°N, 4.5° E) is located inside the winter deep convection area in the
136 Gulf of Lion. It is equipped with a Technicap PPS-3 sediment trap (collection area of 0.125 m²,
137 12 collecting cups of 260 ml) located at a depth of 2400m. The series comprises 80 samples
138 collected between 2011 and 2018 with a collection period from 14 to 28 days. The sampling
139 bottles were filled with 0.45 µm filtered seawater containing sodium borate-buffered formalin
140 (for a final concentration of 5% formalin) to prevent microbial dissolution. After recovery, the

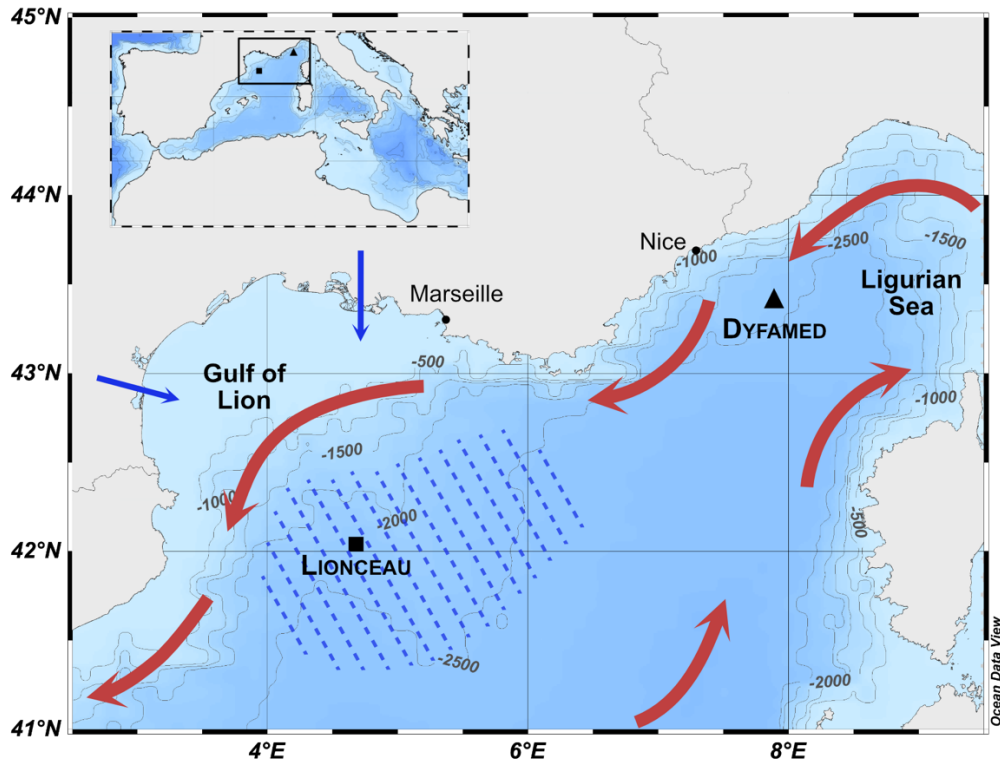


Figure 1. Oceanographic setting of the sediment traps in the NW Mediterranean Sea. The main boundary currents (Northern Current and Western Corsica Current) are represented by the red arrows, the main wind directions (Tramontane and Mistral) by the blue arrows, and the deep convection zone in dashed lines.

141 large “swimmers” were removed by hand, and the remaining particles were either kept in the
 142 formalin solution in cold chambers, or filtered through 0.45 μm pore size membranes, rinsed
 143 and dried at 40°C. Particulate organic carbon (POC) measurements made using an elemental
 144 analyzer were available for the sediment trap samples, and described in Durrieu de Madron et
 145 al. (2017).

146 The sediment trap at the DYFAMED mooring site (43.25°N, 7.52°E) is a PPS-5 Technicap
 147 (collection area of 1 m² and 24 collecting cups) positioned at a depth of 1000m. We analyzed
 148 219 samples collected between 2010 and 2020 with an average sampling period of 15 days. A
 149 detailed description of the sediment processing used at the Dyfamed sediment trap can be
 150 found in Heimbürger et al. (2013). The collecting cups are filled with a solution of 5% buffered
 151 formaldehyde in 0.22 μm -filtered seawater. After retrieval from the trap, samples were kept in
 152 the dark at 4°C. Swimmers were manually removed, and the sediments not analyzed for
 153 particular analyses were rinsed in Milli-Q water, centrifuged and lyophilized. Despite evidence
 154 for lateral inputs into the 1000m sediment trap (Miquel et al., 2011), DYFAMED is often
 155 presented as a site of “open-sea” conditions because of the presence of a hydrological front
 156 disconnecting it from the coast, although continental inputs have been at times documented in
 157 the wintertime (Miquel et al., 2011).

158

159 **2.2 Image acquisition**

160 We used the random settling method to obtain microscope slides from the sediment trap
161 samples (Tetard et al., 2020): a couple of milligrams of the dried sediments were resuspended
162 in water and lightly ultrasonicated for a minute to remove the major aggregates. Around 3 ml of
163 the suspension was then collected and left to settle for four hours on 12 mm × 12 mm cover
164 slips of known mass placed in a 3D-printed decanter (Tetard et al., 2020). The excess water was
165 removed by pipetting, and the decanter was dried overnight at 50°C. The cover slips were
166 weighed, then fixed by sets of eight on a single microscope slide using Norland Optical Adhesive
167 81. The sample slides were mounted on a Leica DMR6000 B automated transmitted light
168 microscope.

169 Each sample was imaged twice with a Hamamatsu ORCA-Flash4.0 LT camera: once using
170 bidirectional circular polarized light to image coccolith calcite, and a second time using
171 brightfield microscopy to image siliceous biominerals, which are amorphous. Coccolith imaging
172 was achieved using a HCX PL FLUOTAR 100× Leica lens. A 561 nm (green) monochromatic
173 bandpass filter (ZET561/10X from Chroma Technology Corp.) was fitted onto the microscope to
174 image a broad range of coccolith thicknesses (Beaufort et al., 2020). We acquired images for
175 around 150 fields of view (FOVs, with dimensions of 125 μm × 125 μm) for each sample using a
176 LabVIEW (National Instruments) interface. Hyperfocused stacks were created from 15 images
177 obtained at different focal depths using the Helicon Focus 7 software (Helicon Soft), which
178 enables to merge into a single image the focused parts of the image stack. Images for opal-
179 bearing phytoplankton particles were obtained with 630× magnification using a HCX PL
180 FLUOTAR 63× Leica lens. Fifteen images (210 μm × 210 μm) were taken and stacked for around
181 250 FOVs to image a depth of at least 15 μm.

182

183 **2.3 Image analysis**

184 The image acquisition step enables to collect two separate sets of images per sample (polarized
185 and brightfield), with each image containing multiple instances of biological fragments. For an
186 approximate number of 150 focused images per sample and two steps of image acquisition, the
187 total number of images used in this study is around 90,000. Deep-learning algorithms proved to
188 be an efficient way to analyze these images (Beaufort & Dollfus, 2004; Godbillot et al., 2024),
189 with a detection step followed by an identification step. Coccolith detection and identification is
190 achieved using SYRACO (Beaufort & Dollfus, 2004), a CNN-based software based which crops
191 then identifies specimens belonging to 33 groups of coccolithophore taxa using images taken in
192 cross polarized light (Beaufort et al., 2022). On the other hand, images for siliceous biominerals
193 were analyzed using a two-step CNN-based protocol: microfossil detection was achieved using a
194 Faster R-CNN trained on a ResNet50 backbone, which achieves 0.74 recall and 0.72 precision
195 (Godbillot et al., 2024). The second step consists in obtaining class counts from the detected
196 images using a classification model. For the purpose of this work, we tested different model
197 runs using the software ParticleTrieur (Marchant et al., 2020). The models were run using

198 13675 images classified into 65 categories, including categories for debris or non-biogenic
199 material. Due to fragmentation and to the use of stacked images, most diatom classes could not
200 be resolved to the species. As a result, the images are mostly resolved to the genus, or
201 attributed to a morphospecies (**Figure 2**).

202 The best model outputs were obtained using a ResNet50 which uses cyclic gain (**Figure S1**), 20
203 ALRS-epochs, 25 minimum images per category, and class weighing. Overall results for this
204 model are 81.0% for precision, 83.8% for accuracy, and 82.2% for recall. For both coccoliths and
205 diatoms, we performed a manual check for all categories, especially for the classes that appear
206 the least in the images, which can be more affected by precision problems than the groups
207 most represented in the dataset.

208 In addition to image classifications, we produced size estimates for each fossil image. For the
209 coccolith images, we used the outputs from the SYRACO software, which uses a series of
210 thresholding techniques to segment the coccoliths from the image background (Beaufort et al.,
211 2022). For the opal-bearing species, for which the use of thresholding techniques was less
212 efficient, we used a U-Net CNN which uses a ResNet43 backbone trained for image
213 segmentation, to generate an outline for the individual particles (**Figure 2**). For each biological
214 class considered, the size reported in this study corresponds to the major axis length.

215

216 **2.4 Particle fluxes to the trap**

217 We generated count data for the categories for which the model exhibits over 80% precision
218 and recall. Count data for each morphospecies was transposed to a flux per day per square
219 meter of a given species (F_i in $\text{day}^{-1} \cdot \text{m}^{-2}$) as follows:

$$220 \quad F_i = \frac{N_i \times A_{\text{slide}} \times m_{\text{trap}}}{N_{\text{image}} \times A_{\text{image}} \times m_{\text{sample}} \times \Delta_t \times A_{\text{trap}}}$$

221 Where N_i is the counts per morphospecies in a sample, A_{slide} the area of the slide in m^2 , m_{trap} the
222 mass of sample collected in the trap, N_{image} the number of images kept for analysis for the
223 sample, A_{image} the area of each image in m^2 (which depends on the lens used during image
224 acquisition), m_{sample} the mass of the sample collected on the slide, Δ_t the collection period of the
225 trap (in days) and A_{trap} the surface area of the trap in m^2 .

226 In addition to particle fluxes to the traps, we derived coccolith- CaCO_3 fluxes to the trap using
227 the methods published in Beaufort et al., 2020 and detailed in the Supplement.

228

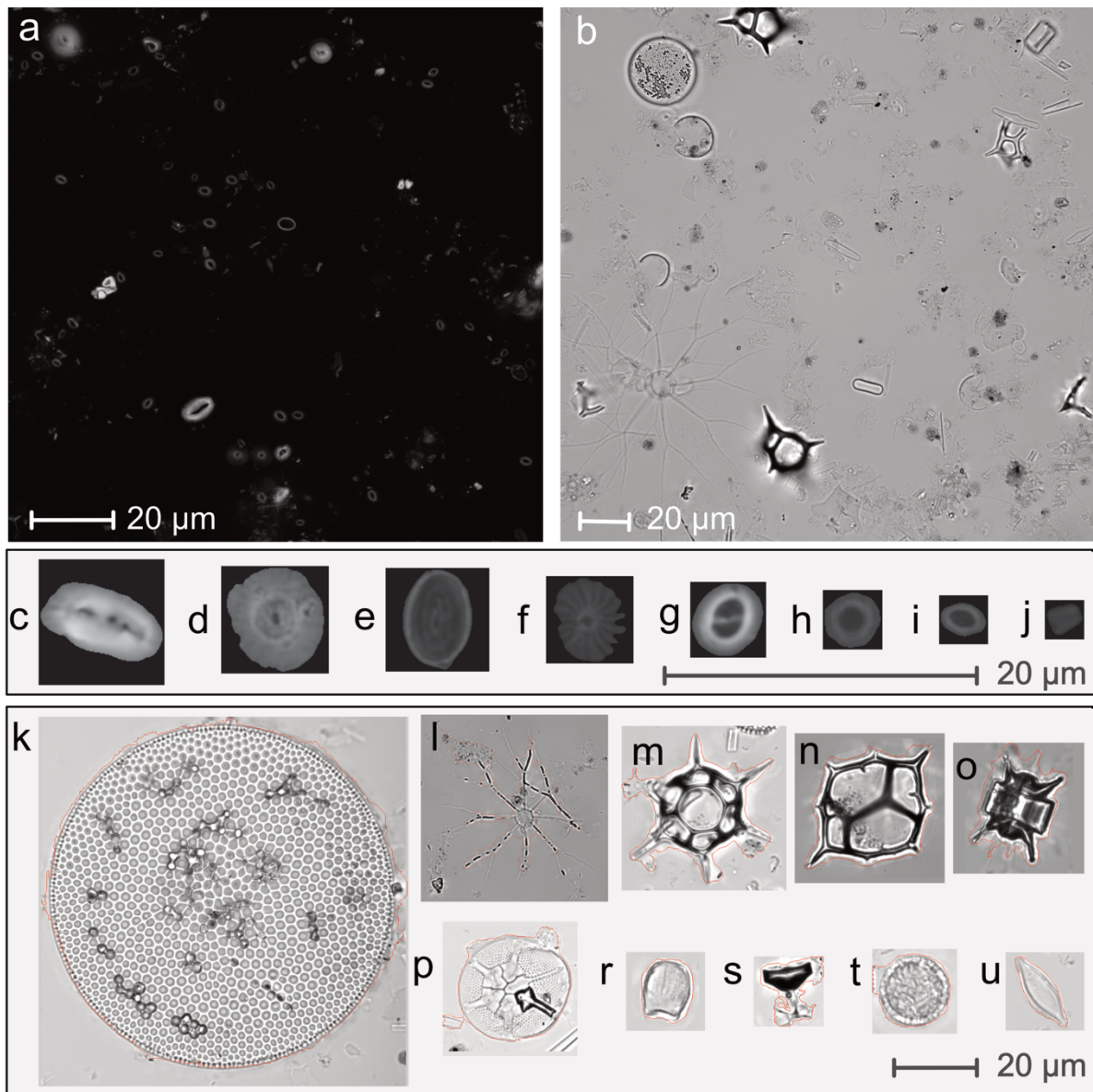


Figure 2. Image acquisition and analysis results. a. Stacked image for sample 609 of the Lionceau sediment series in cross-polarized light. b. Stacked for the same sample using brightfield microscopy. c-j: examples of segmented crops for the morphospecies counted using the SYRACO workflow. k-u: example crops from brightfield microscopy; segmentation results are shown in red. c. *Helicosphaera*, d. *Calcidiscus*. e. *Syracosphaera*. f. *Umbellosphaera*. g. *G. oceanica*. h. *Umbilicosphaera*. i. *Emiliana huxleyi*. j. *Florisphaera profunda*. k. *Thalassiosira*-like. l. *Bacteriastrium*. m. *Dichytocha speculum*, n. *Dichytocha sp.* o. *Odontella sp.* p. *Asteromphalus sp.* r. *Scyphosphaera sp.* s. Resting spore. t. *Calcisphere*. u. *Navicula*-like.

231

232 **2.5 Environmental parameters**

233 We compared the biological production and the carbon fluxes to the two sediment traps to the
234 different environmental variables available for the two sites. The Lionceau sediment trap is
235 located close to the LION mooring line, located in the deep convection area. This line was
236 equipped with 25 instruments (Houpert et al., 2016) which yield results for temperature,
237 salinity and dissolved oxygen over the period considered (Bosse et al., 2023). We also retrieved
238 data for nutrients and the carbonate system, including pH and alkalinity, from the different
239 MOOSE and MOOSE-GE cruises which took place in the region during the period considered
240 (Coppola, 2016; Coppola & Durrieu De Madron, 2020; Coppola & Testor, 2019; Testor, 2017;
241 Testor et al., 2010, 2011, 2012, 2013, 2014, 2015; Testor & Coppola, 2018). The dataset was
242 collected from Sea Data Net (<https://www.seadatanet.org/Data-Access>, last access July 9th
243 2024). The different points sampled and the corresponding year are shown in **Figure S2**. We
244 studied the environmental data for bottles recovered less than 50m deep. Values for
245 temperature at the Lionceau site are retrieved from the CTD sensor which is closest to the
246 surface but still around 150 m deep. DYFAMED, on the other hand, has been subjected to
247 monthly cruises performed on the *RV Téthys II* since 1991. The site has been integrated into the
248 MOOSE network since 2010. During these cruises, CTD profiles are performed and the water
249 column is sampled using 12L Niskin bottles for the analysis of nutrient concentrations and
250 carbonate system parameters (Coppola et al., 2024).

251

252 **2.6 Statistical analyses on taxa-specific relative abundances**

253 Since coccolith fluxes do not directly represent coccolithophore cell fluxes, we used the species-
254 specific average number of coccoliths per coccosphere, as reported in the literature, to
255 calculate coccosphere fluxes (**Table S1**) in the statistical analyses. To address the dominance of
256 certain taxa and reduce the potential influence of skewed distributions, we applied a log-
257 transformation to the relative contributions (in %) of the taxa from both groups. This
258 transformation helps stabilize variance and ensures a more balanced representation of all taxa.
259 Subsequently, we standardized the data by subtracting the mean and dividing by the standard
260 deviation for both seasonal and interannual analyses.

261 To study the seasonal variations of the assemblage at each site, we derived a Principal
262 Component Analysis (PCA) from the monthly averages of the fluxes for the taxa considered.
263 Interannual variations in the phytoplankton assemblage were studied by using the trend in the
264 relative contributions for each species. Because seasons and years were not homogeneously
265 represented in the sediment trap dataset, we first reconstructed the missing flux values using
266 the “stlplus” package on R (Hafen, 2016), which performs a Season-Trend decomposition using
267 Loess (STL) on a time series with missing data. We used this method on the logged and scaled
268 data of the relative abundance of each taxon to extract values for trends for each year-month
269 pair. We used the values for trends to perform a PCA analysis. We also used this decomposition
270 method to associate trend values for each environmental variable to the biological dataset. We

271 then used the “vegan” package (Oksanen et al., 2001) to fit environmental vectors onto the
272 phytoplankton-derived PCA ordination.

273

274 **3 Results**

275 The study of the images obtained using both polarized light and brightfield microscopy yielded
276 counts for a total of thirteen morphospecies of coccoliths, seven morphospecies of diatoms,
277 two dinoflagellates (one calcareous, the other siliceous) and two silicoflagellate morphospecies
278 in the two sediment trap series. Counts for the high-relief and birefringent *Helicosphaera*
279 *carteri* coccoliths were obtained using both image analysis workflows: a comparison of the
280 fluxes measured for each sample using both methods shows that the counts obtained using
281 these workflows are consistent (**Figure S5**).

282

283 **3.1 Total monthly fluxes to trap**

284 In the Ligurian Sea, the maximum particle fluxes of phytoplankton particles toward the
285 DYFAMED sediment trap were recorded in May (7.41×10^8 part.m⁻².d⁻¹), with a notable
286 secondary peak in September (3.83×10^8 part.m⁻².d⁻¹, **Figure 3**). Monthly phytoplankton fluxes
287 for the Lionceau sediment trap were, in average, 20 times more important than at the
288 DYFAMED site. Maximum values were measured in March (3.40×10^{10} part.m⁻².d⁻¹) in the Gulf of
289 Lion and did not display a second peak in the fall.

290 When considering group-specific monthly variations in fluxes, it appears that coccolithophore
291 fluxes were higher than diatom, dinoflagellate and silicoflagellate fluxes at both sites, even
292 when considering the estimates for whole coccolithophore cells (**Figure 4**). In the Ligurian Sea,
293 the maximum fluxes for coccoliths to the sediment trap occurred around the month of May,
294 with a second, smaller peak in September. The opal-forming species displayed a unimodal
295 distribution centred in summer: their peak export was delayed relative to coccoliths, occurring
296 in June in the case of diatom frustules, and July for silicoflagellates. Similar to coccoliths,
297 calcareous dinoflagellates displayed a bimodal distribution, with a first peak in April and a
298 second, more pronounced peak, in the late Summer.

299 Maxima for all biomineral fluxes in the Gulf of Lion occurred earlier than in the Ligurian Sea.
300 The peak for coccoliths occurred in March, along with the opal-forming species and calcareous
301 dinoflagellates. There was a small increase in diatom, silicoflagellate and calcareous
302 dinoflagellate fluxes in June at the site which did not appear in the coccolith group (**Figure 4**).

303

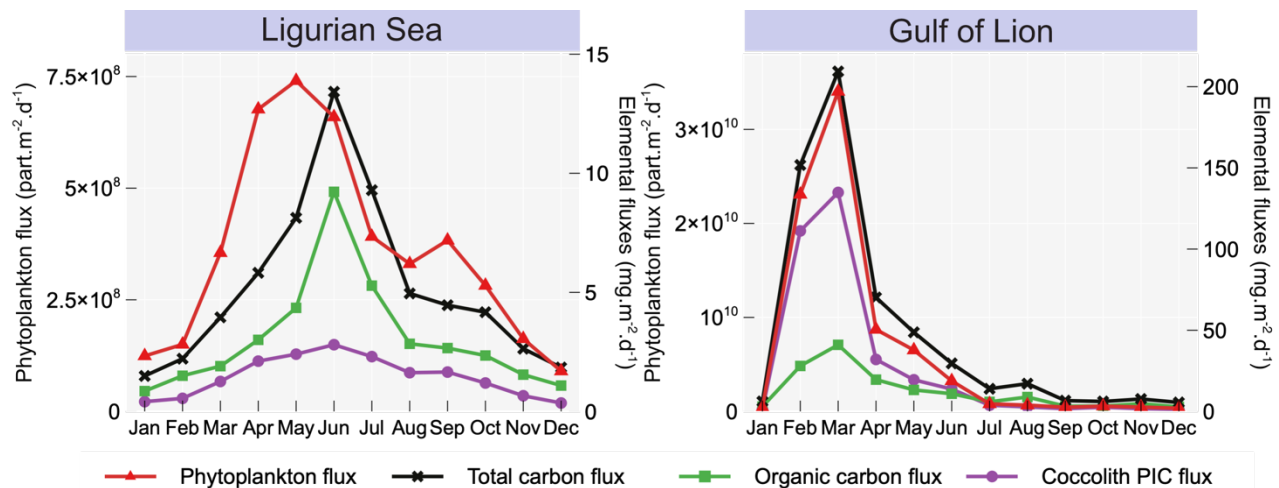


Figure 3 – Average monthly fluxes recorded by the traps. The phytoplankton flux represented here is the sum of coccoliths, diatoms, calcareous dinoflagellates and silicoflagellates, expressed in particles.m⁻².d⁻¹.

304

3.2 Monthly phytoplankton assemblages in the NW Mediterranean Sea

305 Species within a given phytoplankton group exhibit distinct monthly variation patterns,
 306 highlighting differences in phenology among taxa (**Figure 4**). The phytoplankton space was
 307 investigated using only the species present as more than 0.5% of the coccolith assemblage, and
 308 present as more than 0.02% of the assemblage for the remaining categories (*i.e.* diatoms,
 309 silicoflagellates and others). Thus, the analysis for species-specific variations was achieved
 310 considering the following twelve morphospecies: for coccoliths: *Emiliana huxleyi*, *Florisphaera*
 311 *profunda*, *Gephyrocapsa oceanica*, *Helicosphaera carteri*, *Syracosphaera sp.* For diatoms, we
 312 considered *Navicula*-like, *Bacteriastrum sp.*, resting spores and *Thalassiosira*-like cells. We also
 313 considered the silicoflagellates *Dicthyocha fibula* and *Dicthyocha speculum*, as well calcareous
 314 dinoflagellates (both the genii *Thoracosphaera* and *Calciodinellum* have been described in the
 315 area).

316

317

318

319

320

321

322

323

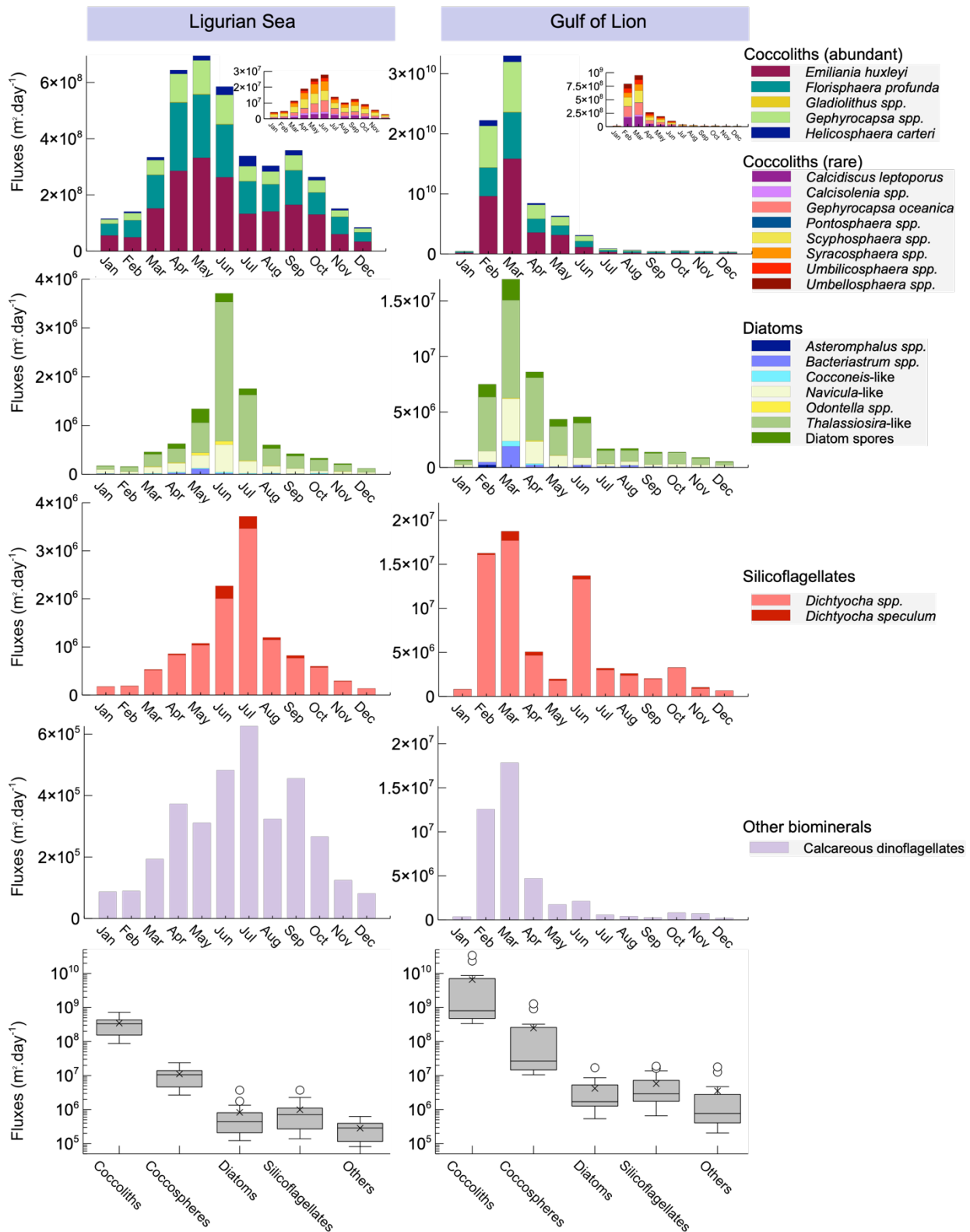


Figure 4 – Monthly fluxes to the trap averaged over the study period for all phytoplankton morphospecies considered in this study. Bottom panels are whisker plots built using the sum of the average monthly values of the morphospecies in each group (e.g. 12 values for each boxplot). Values for coccolithophores are expressed both in coccoliths and coccospheres for comparison.

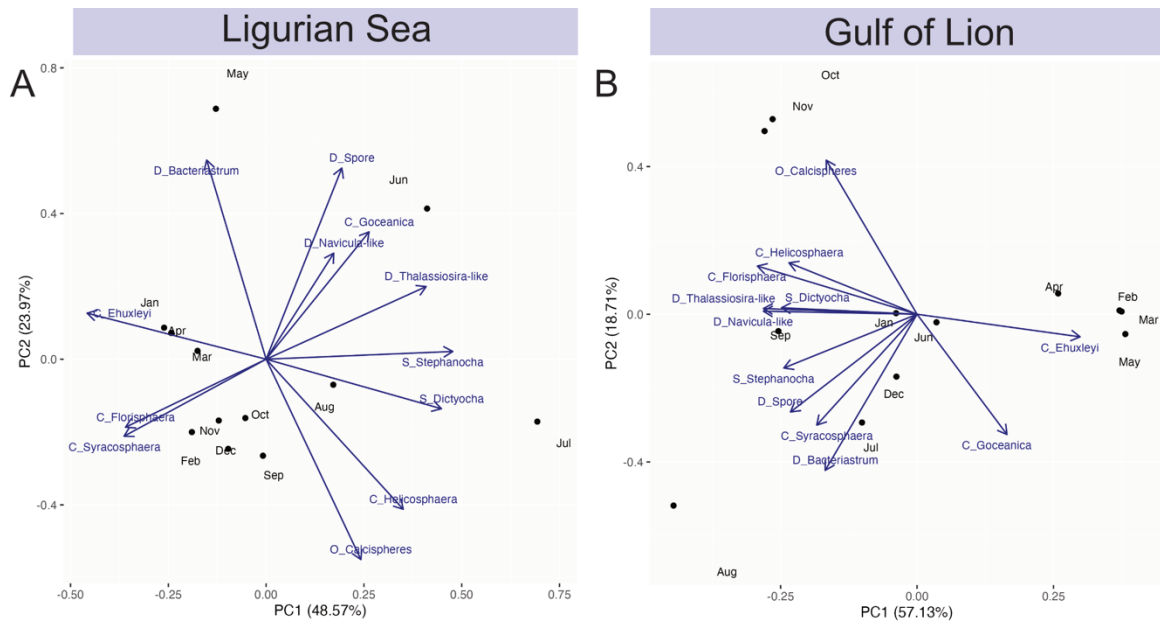


Figure 5 – Monthly variations in the biological particle fluxes to the trap. Principal component analysis (PCA) of the monthly relative assemblage for (A) the DYFAMED series and (B) the Lionceau series.

325 *Emiliana huxleyi* dominated the coccolith assemblage at both sites, along with *Florisphaera*
 326 *profunda* and, to a lesser extent, *Gephyrocapsa sp.* The relative contribution of *Emiliana*
 327 *huxleyi* to the total microfossil assemblage was high throughout the year in the Ligurian Sea
 328 (Figure S7), and dominated the assemblage in the winter and early spring (Figure 5). The
 329 diatom genus *Bacteriastrum sp.* peaked in May. The assemblage then moved to being
 330 dominated by diatom spores (mostly from the *Chaetoceros* genus), when the other
 331 morphospecies described in the sedimentary assemblage seemed to generally decrease (Figure
 332 S7). June was marked by an increase in the small but rather calcified *Gephyrocapsa oceanica*,
 333 along with the large centric diatoms grouped under “*Thalassiosira-like*” that dominated the
 334 diatom assemblage, and smaller pennate diatoms grouped under “*Navicula-like*” (Figures 5,
 335 S7). These morphospecies were followed by an increase in both silicoflagellate categories and
 336 the heavily calcified *Helicosphaera carteri* and calcareous dinoflagellates. Finally, fall conditions
 337 were mostly dominated by coccolithophores from the *Florisphaera profunda* species and
 338 *Syracosphaera sp.*

339 The Lionceau sediment trap displayed a similar biological succession although the
 340 corresponding months can precede those observed at DYFAMED by 2-3 months. *Emiliana*
 341 *huxleyi* dominated the assemblage in the mid-winter and spring. These were periods where
 342 other Noelaerhabdaceae species were also abundant in the assemblage, including
 343 *Gephyrocapsa oceanica* and *Gephyrocapsa sp.* (Figures 5, S8). In July, the assemblage was
 344 dominated by the diatom *Bacteriastrum*, although this was rather due to a decrease in the
 345 numbers of Noelaerhabdaceae coccoliths reaching the seafloor than because of an increase in

346 this diatom's occurrence. The succession in diatoms was then similar to the one observed in the
347 Ligurian Sea: diatom spores dominated in late August, *Thalassiosira*-like and *Navicula*-like in
348 September, together with silicoflagellates. The heavily calcified *Helicosphaera carteri* and
349 calcareous dinoflagellates were last to appear in this succession in October to November.
350 *Florisphaera profunda* occurred simultaneously to these species, dominating the assemblage in
351 the fall (**Figures 5, S8**).

352

353 3.3 Interannual variations in fluxes, relative assemblages and size

354 At DYFAMED, the maximum fluxes and the minimum fluxes were recorded respectively in May
355 2013 (3.02×10^9 part. $m^{-2}.d^{-1}$) and January 2018 (6.45×10^6 part. $m^{-2}.d^{-1}$). Maximum and
356 minimum phytoplankton fluxes toward the sediment trap were recorded respectively in
357 February 2012 (1.82×10^{11} part. $m^{-2}.d^{-1}$) and January 2017 (1.48×10^8 part. $m^{-2}.d^{-1}$) at the
358 Lionceau site.

359 In general, total biological fluxes to the seabed decreased in the NW Mediterranean Sea over
360 the period of study (**Figure S6**), as did most species-specific fluxes (**Figures 6, S9, S10, S11**). The
361 decrease in total particle fluxes was more marked in the Gulf of Lion than in the Ligurian Sea
362 (**Figure S6**). In the Ligurian Sea, the decrease in fluxes was more apparent for opal-forming
363 species than for calcareous phytoplankton: *Navicula*-like and *Thalassiosira*-like are the classes
364 where fluxes decreased the most (**Figure S11**), while most coccolithophore species were
365 preserved. In the Gulf of Lion on the other hand, calcifying species were most affected by the
366 decrease in fluxes: *Helicosphaera carteri* displayed the steepest decline, and calcareous
367 dinoflagellates also displayed a sharp decrease. Opal biominerals were less affected by the
368 decline, or displayed, in the case of *Bacteriastrum* sp. and *Navicula*-like, increased fluxes to the
369 sediment trap during the period of study (**Figures 6, S11**).

370 Relative assemblages also varied during the period of study. In the Ligurian Sea, the two PCA
371 axes represented 60% of the changes in relative assemblages across the period of study (**Figure**
372 **7**). The first PCA loading increased throughout the interval, which was due, in particular, to an
373 increase in the number the species *Florisphaera profunda* and *Syracosphaera* sp. in the relative
374 assemblage, while opal-bearing species such as *Bacteriastrum* sp., *Navicula*-like and *Dichtyochoa*
375 *speculum* decreased. In the Gulf of Lion, the first two axes gathered 70% of the changes in the
376 relative assemblage. The changes are mainly explained by a decrease in coccoliths from the
377 Noelaerhabdaceae family in the assemblage, whereas most opal-forming species (including
378 *Thalassiosira* and *Navicula*-like, the two silicoflagellate categories, etc.) increased (**Figure 7**). At
379 both sites, these changes were most correlated to an increase in temperature and a decrease in
380 pH. A second source of variation in the Gulf of Lion, shown by the decrease along the second
381 axis of the PCA during the study period, is related to a general increase in *Florisphaera profunda*
382 and *Syracosphaera* sp. in the assemblage between 2011 and 2018.

383

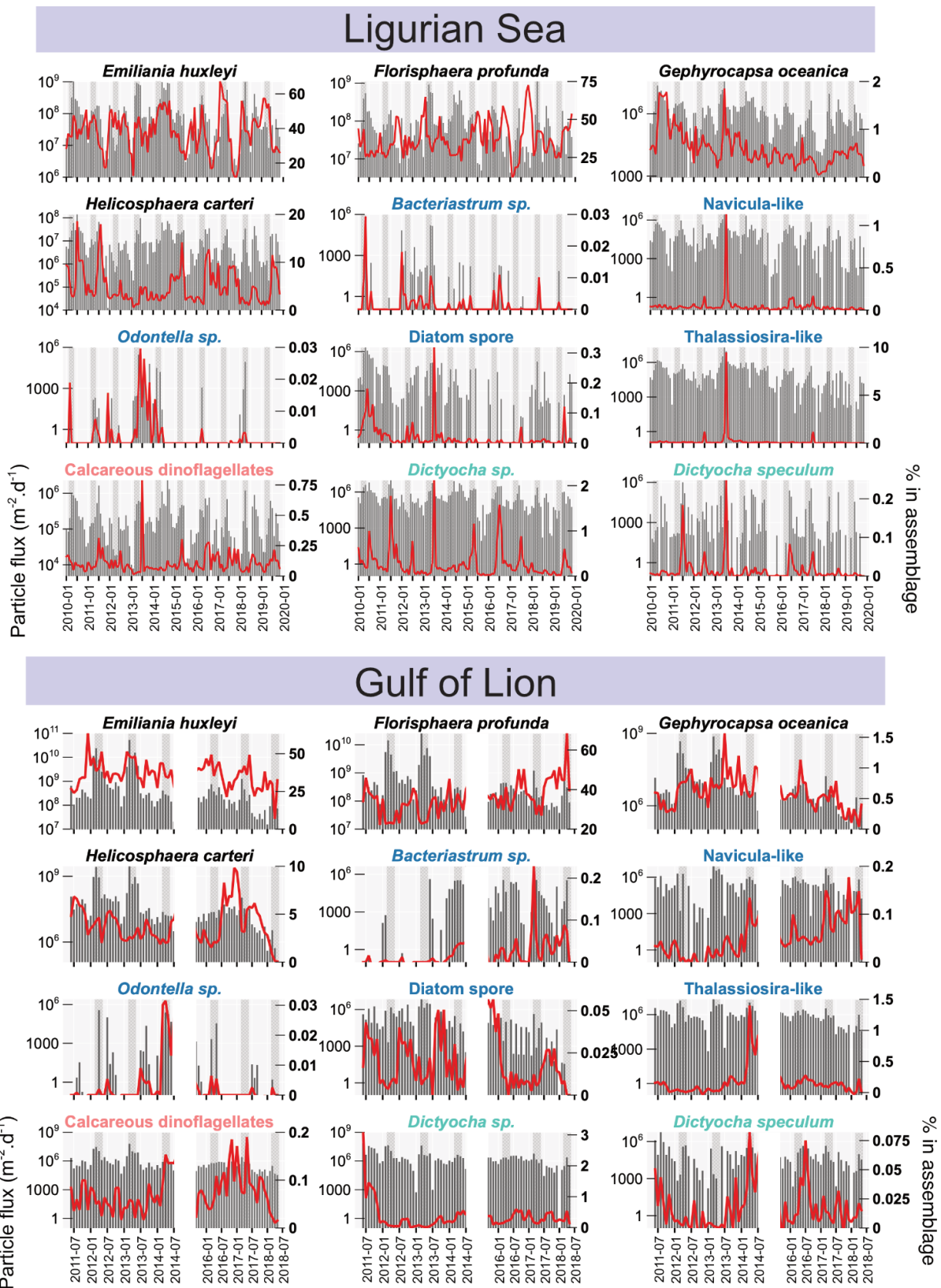


Figure 6. Interannual variations in species-specific monthly fluxes and relative contribution to the assemblage. The relative presence of the species in the assemblage is represented by the red line, and the fluxes by black bars. Overall fluxes for all species considered here decrease over the period of study. See Methods for details on how missing monthly values were reconstructed. Note the interruption in the Lionceau series in 2015.

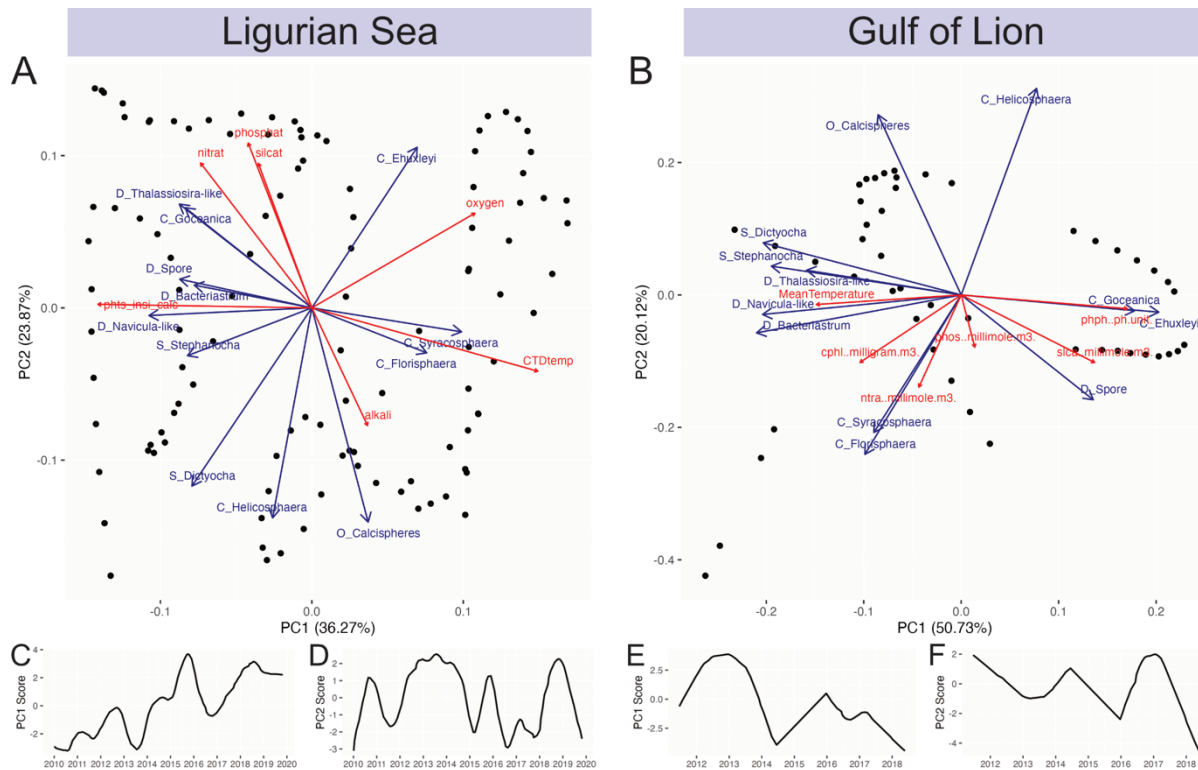


Figure 7: Interannual variations in the phytoplankton assemblage. Principal component analysis (PCA) of the relative assemblage trends for (A) the DYFAMED series and (B) the Lionceau series. The trends in the different environmental variables are projected on the PCA. (C; D) are PCA 1 and PCA 2 individual data points coordinates for DYFAMED, and (E; F) are for Lionceau.

385 across the period of study. It appears that size variations were quite restricted during the
 386 period of study at both sites (**Figures S12, S13, S14**). The largest size changes in the Ligurian Sea
 387 may be attributed to *Thalassiosira*-like diatoms and the silicoflagellates *Dichyocha* *sp.*, which
 388 both increased slightly over the period of study. In the Gulf of Lion *Florisphaera profunda* and
 389 *Dichyocha speculum* both increased during the period of study, while both *Emiliania huxleyi*
 390 and *Navicula*-like decreased over the interval, with a steep decline occurring after 2015 in both
 391 cases.

392

393 4 Discussion

394 4.1 Impact of post-depositional processes on the particle export to trap

395 The average monthly flux for coccoliths in the Ligurian Sea during the study period was 3.47
 396 $\times 10^8$ part.m⁻².d⁻¹, which is comparable to the fluxes recorded at the nearby Planier sediment
 397 trap (6.1×10^8 coccoliths.m⁻².d⁻¹) located off the coast of Marseille at a depth of ~500m (Rigual-
 398 Hernández et al., 2013). This value is also similar to the maximum fluxes reported for a
 399 sediment trap located in the central eastern Mediterranean Sea (Ziveri et al., 2000) at 3000m

400 depth (3×10^8 coccoliths.m⁻².d⁻¹). By comparison, the Lionceau sediment trap recorded
401 significantly higher coccolith monthly fluxes, averaging 6.61×10^9 coccoliths.m⁻².d⁻¹.

402 Calcareous dinoflagellates also made up an important component of the calcareous particles
403 identified in the sediment trap series. Average monthly fluxes were 3.53×10^6 part. m⁻².d⁻¹ in the
404 Gulf of Lion and 2.84×10^5 part. m⁻².d⁻¹ in the Ligurian Sea respectively, representing
405 respectively 54 and four times the fluxes reported for the Eastern Mediterranean Sea. Average
406 daily silicoflagellate fluxes recorded at DYFAMED are 0.3 higher than at the Planier site and 0.2
407 those recorded at the Lacaze-Duthier sediment trap located at 500m depth (Rigual-Hernández
408 et al., 2010).

409 In contrast to these biominerals, diatom valve fluxes were markedly lower in this study
410 compared to the coastal Planier site. The Planier sediment trap recorded average diatom fluxes
411 (3×10^7 valves.m⁻².d⁻¹) that were seven times higher than in the Gulf of Lion (5.8×10^6 valves.m⁻².d⁻¹
412 in average) and 36 times the average flux measured in the Ligurian Sea (9.9×10^5 valves.m⁻².d⁻¹).
413

414 Thus, diatom fluxes appear depressed relative to the other phytoplankton particles identified in
415 the traps, in comparison to similar existing studies. This could reflect either nutrient-depleted
416 conditions in the Gulf of Lion and Ligurian Sea, or differences in their preservation.
417 Coccolithophores are nutrient stress-tolerant species (S-strategists) (Brun et al., 2015). The
418 nutrient-depleted conditions that prevail in the Mediterranean Sea can explain, in part, their
419 overwhelming presence in the record. Additionally, the circular shape and organic matter
420 coating of coccoliths is likely to enhance their preservation in the sediments (Hassenkam et al.,
421 2011). Conversely, diatoms, which are less well-preserved due to their silica-based frustules'
422 susceptibility to dissolution, may contribute to an overrepresentation of coccolithophores in
423 the samples. The most abundant diatom taxa identified at the Planier sediment trap, which is
424 closer to the surface and to the shore, were *Thalassionema frauenfeldii* and *Skeletonema* sp.,
425 the latter making up more than 43% of the assemblage. In contrast with this coastal site,
426 *Skeletonema* was nearly absent in our samples, and was also absent from superficial sediment
427 samples collected at the Planier site (Rigual-Hernández et al., 2013). *Thalassionema* sp. exists in
428 our dataset but almost exclusively as fragments, for which counts were not used in this study.
429 Resting spores, which made up the third most observed group at the Planier site, were
430 observed in our samples. The high export efficiency of resting spores has been noted before
431 (Rembauville et al., 2015; Riaux-Gobin, 1996; Rynearson et al., 2013), in part due to their
432 robustness. Thus, heavily silicified diatoms appear to be overrepresented in the phytoplankton
433 assemblage in our study, a result which has been documented before for core-top and trap
434 sediments (Abrantes, 1999; Zúñiga et al., 2021).

435

436 **4.2 Drivers of total biological export to the trap and link with carbon export**

437 *4.2.1 Ligurian Sea*

438 The collection of sinking particles in sediment traps can be affected by the sinking particle
439 concentrations and velocities (Buesseler et al., 2007). Previous studies on the DYFAMED

440 sediment trap have shown that stable and weak hydrodynamic conditions ensure the trap's
441 efficiency. Under the conditions prevailing at the site, the particles produced in the surface
442 typically reach the 1000m-trap in approximately two weeks (Miquel et al., 2011).

443 Phytoplankton fluxes to the sediment trap in the Ligurian Sea exhibit a bimodal distribution,
444 reflecting the presence of a spring and autumn bloom at the site, a documented feature in the
445 NW Mediterranean Sea (Mayot et al., 2020; Rigual-Hernández et al., 2013). The spring bloom is
446 generally triggered between March and May, when increasing stratification in the surface
447 concentrates the nutrients replenished by winter mixing in the photic zone. The autumn bloom,
448 on the other hand, occurs between September and November, when the breakdown of
449 summer stratification enables some nutrients to reach the surface.

450 Our study highlights that the maximum fluxes of organic matter to the trap in June occur
451 approximately one month after the maximum flux of biological particles. A similar lag had been
452 observed between total mass fluxes and organic carbon fluxes at this trap series before, and
453 had been attributed to the production of material with higher organic carbon content in the
454 late spring (Miquel et al., 2011). Our results suggest that this lag is caused by the export of
455 different particles at depth. In the sedimentary assemblage, coccolithophores are an important
456 component of the spring peak in fluxes, with coccoliths making up more than 90% of what
457 reaches the seafloor in the spring, a number that remains generally above 80% if we consider
458 for example that a single coccosphere is made up of 50 coccoliths. Coccolith production does
459 not appear to be responsible for burying organic carbon at the site: instead, peak organic
460 carbon fluxes at the site are reached in the late spring, when opal-bearing species from the
461 diatom and silicoflagellate groups dominate the assemblage. Similarly, the increase in
462 coccoliths in the sediment trap samples in the autumn is not accompanied by an increase in
463 POC. This may provide an explanation as to why the autumn bloom does not contribute
464 significantly to the annual export of organic carbon from the surface, as noted by Miquel et al.
465 (2011).

466 Interestingly, the peak in total coccolithophore fluxes to the DYFAMED trap are not correlated
467 to the Particulate Inorganic Carbon (PIC) fluxes represented by coccoliths calculated using our
468 workflow (Beaufort et al., 2020). The maximum coccolithophore fluxes are found during the
469 spring, with *Emiliana huxleyi* dominating the assemblage. PIC fluxes, on the other hand are
470 maximum during the summer, at a time when *Helicosphaera carteri*, a larger and very calcified
471 species, increases both in total and relative abundance in the sedimentary assemblage. Thus,
472 this species seems to drive PIC burial in this region of the Mediterranean Sea.

473 4.2.2 Gulf of Lion

474 In the Gulf of Lion, the biological fluxes to the trap display a unimodal distribution that matches
475 the one observed at the coastal Planier sediment trap (Rigual-Hernández et al., 2013).
476 However, the average coccolith fluxes at the site (1.0×10^{10} coccoliths.m⁻².d⁻¹) are an order of
477 magnitude higher than reported at this coastal site, and seven times the average flux reported
478 in the Canaries, in an area affected by coastal upwelling episodes (Sprengel et al., 2000). In the
479 Gulf of Lion, the maximum fluxes coincide with episodes of winter convection. Similar to
480 regions such as the Greenland Sea, the NW Mediterranean Sea is a known region of dense

481 water formation. In the winter, cold and dry winds trigger the formation of dense water in the
482 surface, leading to convection events that, on certain years, affect the entire water column
483 (Durrieu De Madron et al., 2013; Houpert et al., 2016; Margirier et al., 2020). Increased
484 biological activity due to deep winter mixing is a general feature in the NW Mediterranean,
485 supplying the surface in nutrients: the 2012 deep convection episode is associated with positive
486 chlorophyll a anomalies in both the Gulf of Lion and the Ligurian Sea in March 2012 (Ciancia et
487 al., 2021), coinciding with the maximum fluxes in biological particles to the trap at Lionceau.
488 Beyond the direct effect on biological production, convection episodes have consequences on
489 particle deposition at depth that may explain why the fluxes exceed those recorded in other
490 series (Stabholz et al., 2013). In 2011, the convection episode was detected between January
491 and March, while the phytoplankton bloom developed at the beginning of March (Severin et al.,
492 2014). *In situ* sampling suggests that the 2011 bloom continued to develop in April after the end
493 of the convection episode, a feature that is absent from our record, where instead biological
494 fluxes to the trap drop after March. At least part of the biological fluxes recorded at the
495 Lionceau trap could thus be attributed to physical processes, such as resuspension episodes.
496 Such events occurred in the winters of 2010 to 2013 during episodes of bottom-reaching
497 convection and the subsequent dispersion phase of the newly formed dense bottom waters
498 (Durrieu de Madron et al., 2017; Severin et al., 2017). They may also be derived from
499 concurrent dense shelf water cascading input, which that has been shown to concentrate
500 biological material (Canals et al., 2006; Pusceddu et al., 2013; Yoder & Ishimaru, 1989). These
501 processes can explain why fluxes at the Lionceau site exceed those observed in the Ligurian Sea
502 and the Canaries.

503 Contrary to the Ligurian Sea, maximum PIC and POC fluxes to the trap in the Gulf of Lion
504 coincide with the total fluxes of biological particles, which are dominated by coccoliths. While
505 deep convection reduces the organic content of the sediments collected in the trap by burying
506 non-organic material (Stabholz et al., 2013), including from resuspension episodes, it is an
507 important means of sequestering carbon at depth (Kessouri et al., 2018). Increased burial of
508 POC during deep convection episodes was linked to increased export efficiency (*i.e.*
509 export/primary production) rather than to increased biological activity in the surface layer
510 (Kessouri et al., 2018).

511 **4.3 Monthly phytoplankton assemblages reflect sea surface conditions**

512 There is a clear monthly succession in the microfossils found in the sediment traps. Similar to
513 the results found at the Planier site (Rigual-Hernández et al., 2013), colder conditions seem to
514 favor coccolithophores from the Noelaerhabdaceae family, with *Emiliana huxleyi* dominating
515 the assemblage in the winter and early spring at both sites. This species is also the most
516 abundant in the assemblage in high-nutrient conditions, which prevail in the winter in the Gulf
517 of Lion when convection events occur, and around the month of April in the Ligurian Sea. The
518 ability of *E. huxleyi* to outcompete other coccolithophore species in high light and eutrophic
519 environments has been documented before (Tyrrell & Merico, 2004). However, the
520 phytoplankton blooms in the region are usually dominated by diatoms rather than
521 coccolithophores (Marty et al., 2002). Our observations do not correspond either to the group
522 succession classical described in mid latitudes ocean (Margalef, 1978) which posits that diatoms

523 typically dominate during periods of high nutrient availability and turbulence, such as in early
524 spring. We explain this apparent paradox by the absence in our dataset of most of the diatom
525 species traditionally associated with the turbulent and nutrient-rich waters that develop in the
526 spring: *Chaetoceros* sp., *Odontella* sp., and *Skeletonema* sp. These weakly-silicified species were
527 likely not preserved in the samples collected from the two trap series we studied, which are
528 located deeper than the one at the Planier site where they were observed (Rigual-Hernández et
529 al., 2013). The secondary peak exhibited by *E. huxleyi* in the late summer (September) in the
530 Ligurian Sea was also noted at the Planier site off the coast of Marseille, whereas it is absent in
531 the Gulf of Lion. This later bloom develops when decreasing temperatures break the
532 pycnocline, enabling nutrient input to the surface. Rigual-Hernández et al. (2013) attribute the
533 absence of diatoms in the assemblage during this period to the weaker mixing and nutrient
534 concentrations which distinguish this second bloom from the spring bloom.

535 Contrary to diatoms, silicoflagellates appear over-represented in sediment trap samples
536 compared to sea surface records, probably due to their robustness. Our record shows that their
537 presence in the assemblage is most associated to warm and nutrient-depleted conditions,
538 similar to *Helicosphaera carteri*, which has been associated to oligotrophic conditions (Keuter et
539 al., 2022; Ziveri et al., 2000). We observe no seasonal difference between the different
540 silicoflagellate morphospecies identified in the sediment trap, an observation previously made
541 in other Mediterranean sediment trap studies (Rigual-Hernández et al., 2010). There is a
542 greater diversity in the phytoplankton community in the summer, which is typical for
543 oligotrophic regimes (Keuter et al., 2022). The summer assemblage at both sites includes large
544 centric diatoms, grouped under *Thalassiosira*-like, which are also most present in the summer
545 assemblage at the coastal Planier site (Rigual-Hernández et al., 2013), as was *Nitzschia*
546 *bicapitata*, which in our dataset is included in the *Navicula*-like group. Calcareous
547 dinoflagellates also peak in the summer. A study by Vink (2004) showed that these species were
548 mostly associated with a stratified upper water column and a well-established
549 thermo/pycnocline.

550 Finally, autumn (October-November) conditions at the sites display contrasted assemblages: in
551 the Ligurian Sea, the assemblage is composed of *F. profunda*, a species known for developing in
552 the lower photic zone under oligotrophic conditions. Similarly, *Syracosphaera* sp., which tends
553 to co-occur in the assemblage, has been associated to the lower photic zone, although this
554 genus is less well documented and diverse (Bown et al., 2009). An increase in *F. profunda*'s
555 relative presence in an assemblage could suggest the presence of very nutrient-depleted
556 conditions in the surface in the Ligurian Sea, a feature that is absent from the record in the Gulf
557 of Lion. Overall, the phytoplankton monthly averages reflect the more oligotrophic conditions
558 present in the Ligurian Sea compared to the deep convection area. The coccolithophore
559 phenology described here aligns with observations from the Gulf of Biscay (Beaufort &
560 Heussner, 2001), which similarly documented *F. profunda* in late fall, *H. carteri* in summer, and
561 *Syracosphaera pulchra* in early fall.

562

563

4.4 A decrease in phytoplankton fluxes in the NW Mediterranean

564 Total phytoplankton fluxes generally decreased at the two sites investigated between 2010 and
565 2018 (**Figure S6**). In the Gulf of Lion, it appears that, contrary to some very robust coccoliths,
566 some fragile elements such as *Bacteriastrum* experience an increase in fluxes across the period
567 of study. This indicates that the state of preservation did not vary during the period of study
568 and suggests that the decrease in fluxes instead reflects changes in primary production in the
569 surface.

570 The total phytoplankton fluxes of the Lionceau series decrease abruptly in 2014 (**Figure S6**). In
571 the Ligurian Sea, the overall decrease in phytoplankton and carbon fluxes is less pronounced.
572 An exception to the decreasing trend occurs between 2013 and 2014 (**Figure S6**), with trends in
573 phytoplankton and carbon fluxes instead displaying an increase. The decrease in phytoplankton
574 total abundance since 2010 has been documented for the NW Mediterranean Sea before, and
575 attributed to the decrease in nutrient concentrations in the sea surface (Garcia et al., 2023).

576 Under present-day conditions, concentrations in chlorophyll a in the NW Mediterranean Sea
577 are correlated to the mixed-layer depth (Macias et al., 2018). Therefore, we suggest that the
578 decrease in phytoplankton fluxes to the sediment traps is linked to the reduction in vertical
579 mixing that affects the region, through its impact on nutrient concentrations. Decreasing
580 phytoplankton fluxes in the Gulf of Lion indeed mirror the environmental changes that affected
581 the water column during the period of study: studies show that unlike the period between 2009
582 and 2013, where the intensification of winds in the winter triggered a deep convection episode,
583 the years between 2014 and 2018 were not affected by a similar phenomenon (Margirier et al.,
584 2020). This absence of deep convection was attributed to reduced winter heat loss in 2014
585 which led the region to transition into a warmer and more saline state lasting until 2018 – a
586 phenomenon that is likely to occur more frequently in the NW Mediterranean Sea, as the air
587 warms more rapidly than the sea surface (Josey & Schroeder, 2023; Parras-Berrocal et al.,
588 2022). In contrast to the Gulf of Lion, deep convection episodes are less frequent in the Ligurian
589 Sea (Macias et al., 2018), although the region experiences vertical mixing in the upper part of
590 the water column. In the period between 2008 and 2018, the winter convection was most
591 intense in 2013 and 2014 (Bosse et al., 2017; Margirier et al., 2020). The decrease in
592 phytoplankton fluxes observed in both sediment trap series thus appear to be closely linked to
593 the decreased mixing conditions in the water column, which reduce the upward flux of
594 nutrients to the surface, and lead to warmer temperatures in the upper water column
595 (Margirier et al., 2020).

596

4.5 Contrasting trends in diatoms and coccolithophores at both sites

597 While both sites exhibit reduced biological fluxes to the sediment traps between 2010 and
598 2018, the study of the phytoplankton assemblages reveals distinct trends. In the Ligurian Sea,
599 coccoliths show an increase relative to diatoms and silicoflagellates in the assemblage (**Figure**
600 **8**). This relative increase of coccoliths in the assemblage is driven mainly by a relative increase
601 in the *Florisphaera profunda* and *Syracosphaera* sp., two groups associated with very nutrient-
602 depleted conditions in the sea surface. A comparison with environmental parameters (**Figure 7**)
603 suggests that these changes are most correlated to a temperature increase and a pH decrease

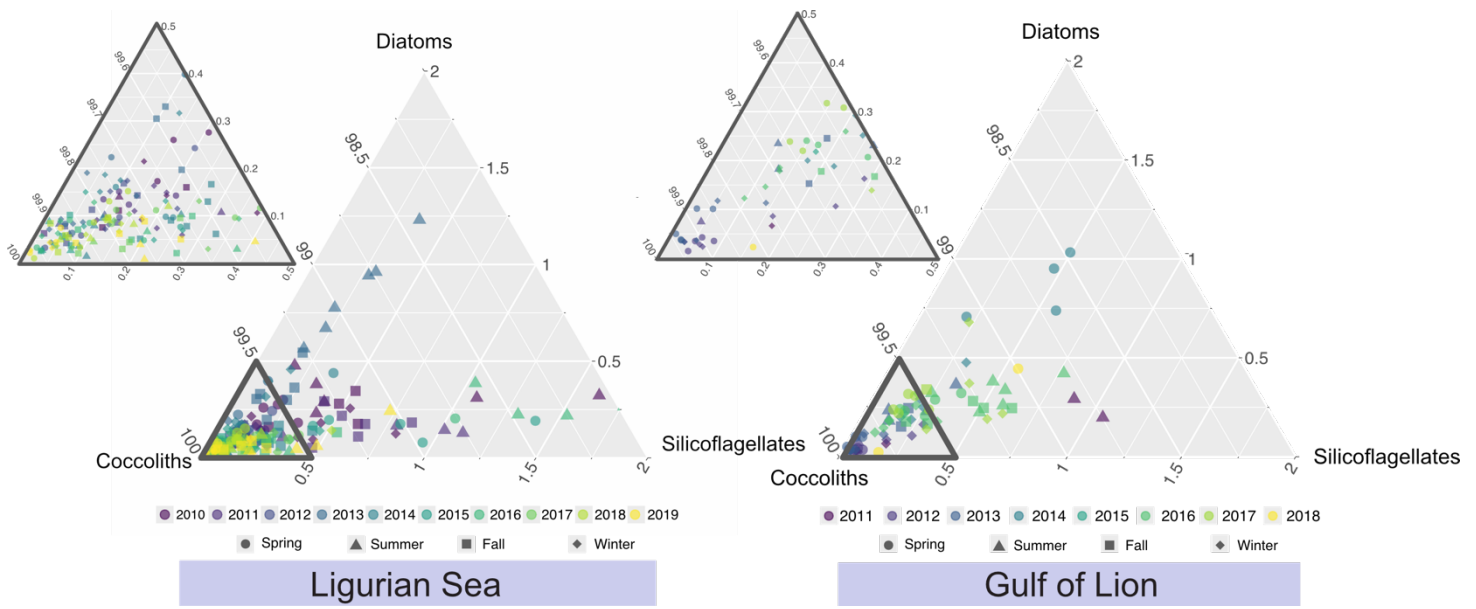


Figure 8 – Ternary plots for the relative contributions of all coccolith, diatom, and silicoflagellate particles to the trap. Points are colored by year. The sites show contrasting trends over the period of study, with coccoliths increasing relative to both diatoms and silicoflagellates in the Ligurian Sea, while the Gulf of Lion displays the opposite trend.

604 in the Ligurian Sea. An increase in *F. profunda* abundances relative to other coccoliths has been
 605 linked to increased temperatures for latitudes above 30°N (Hernández-Almeida et al., 2019),
 606 although the mechanisms for this relationship remain elusive. At DYFAMED, the increase in *F.*
 607 *profunda* % at the site is the result of a (relatively) larger decrease in both diatom and
 608 Noelaerhabdaceae fluxes across the interval (**Figure 6**). Fluxes for opal-bearing species,
 609 especially large centric diatoms, indeed seem to decline faster than those of the carbonate-
 610 producer (**Figure S11**).

611 While the occurrence of the deep-dwelling *F. profunda* and *Syracosphaera* sp. also increases
 612 slightly in the phytoplankton assemblage of the Gulf of Lion (**Figure 7**), the largest trend
 613 observed at this site of deep convection is an increase in diatoms and silicoflagellates
 614 percentages in the assemblage (**Figures 7, 8**). This result converges with the observation that
 615 PIC fluxes are decreasing faster than total carbon fluxes at the site (**Figure S6**), a feature that is
 616 less evident in the Ligurian Sea. While part of this decrease can be attributed to a larger decline
 617 in the fluxes of carbonate-producers, it appears that some opal-bearing classes, namely
 618 *Bacteriastrum* sp. and *Navicula*-like, display increasing fluxes to the trap. Similar to the Ligurian
 619 Sea, these assemblage changes are most correlated to an increase in subsurface temperatures
 620 and to a decrease in pH (**Figure 7**). However, an increase in silicate concentrations is also
 621 correlated to the change, which could explain why the opal-bearing classes appear to increase
 622 in the assemblage. There is a general lack of data for nutrient trends in the open sea, making it
 623 difficult to highlight a causal influence of nutrient changes on the assemblage changes
 624 observed. The Gulf of Lion is the only site in the NW Mediterranean Sea where an increase in
 625 nutrients has been documented for intermediate waters, although this observation concerns

626 nitrates only (Fourrier et al., 2022) and has not been reported for the surface. Alternatively, the
 627 decrease in coccoliths relative to other biological particles at Lionceau could be related to a
 628 decrease in surface pH. The data from the MOOSE cruises suggest that a mean pH drop of 0.2
 629 points (from 8.3 to 8.1) occurred in the Gulf of Lion between 2012 and 2014 (**Figure S3**),
 630 whereas the pH decrease in the Ligurian Sea remained rather limited. Additional data is needed
 631 in the region to corroborate such an abrupt decrease. Nevertheless, other studies have
 632 documented that while the entire Mediterranean Sea is subjected to decreasing pH, the Gulf of
 633 Lion is acidifying at a rate twice as important as the rest of the region (Tsiaras et al., 2024),
 634 including the Ligurian Sea (Fourrier et al., 2022). Acidification has been shown to hinder
 635 calcification for most coccolithophore species in *in vivo* experiments (Meyer & Riebesell, 2015),
 636 and has been shown to impair the bloom-forming abilities of *Emiliana huxleyi* (Riebesell et al.,
 637 2017).

638 4.6 Implications on phytoplankton size structure and carbon burial

639 The size of the phytoplankton community influences carbon cycling in the water column (Jin et
 640 al., 2006). In the Ligurian Sea, the phytoplankton assemblage shows a marked decrease in
 641 larger size categories between 2010 and 2019, while smaller particles experience a slower
 642 decline (**Figure 9**). The Gulf of Lion displays the opposite trend, with fluxes of small particles

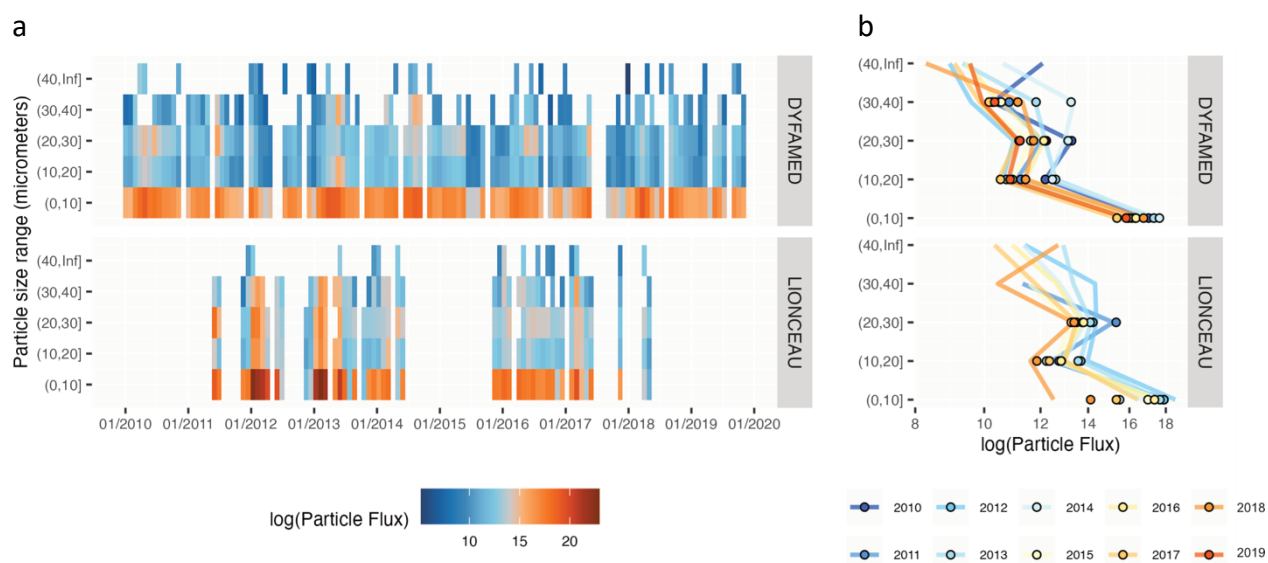


Figure 9 – Size-specific changes in phytoplankton fluxes between 2010 and 2017. Panel a: Color chart for the biological particle fluxes to the trap per size category over time. Small particles (coccoliths) overwhelmingly dominate both assemblages. Panel b: Yearly averages for the fluxes of particles of each size category, per year. Yearly averages were measured using the unmodified data from panel A (lines), and a second time using uninterrupted reconstructed values when the seasonal decomposition method was possible (points). This second method accounts for seasonal biases in fluxes that may be present in the unmodified data. Both methods suggest that while average fluxes are decreasing throughout the size categories, in the Gulf of Lion this decrease is more evident for smaller size classes, effectively increasing the proportion of large biological particles in the assemblage.

643 decreasing more rapidly than those of larger ones, leading to an overall increase in the
644 proportion of larger particles in the assemblage. This observed shift in size structure is not due
645 to species-specific changes in size, as no individual species shows a consistent size trend over
646 the study period (**Figure S13**). Instead, we attribute these changes to variations in the dominant
647 phytoplankton groups. In the Gulf of Lion, the increase in diatoms, generally larger than
648 coccolithophores, contributes to the relative increase in larger particles. Meanwhile, in the
649 Ligurian Sea, the small-sized *F. profunda* coccoliths become more prominent in the assemblage,
650 contributing to the overall decrease in particle size (**Figure 9**). Water column stratification and
651 the resulting nutrient-depleted conditions have been shown to favor small coccolithophores
652 over large diatoms in the Humboldt Current System, inhibiting carbon burial (Iriarte & González,
653 2004). Similarly, in the NW Mediterranean Sea, diatoms appear more efficient at burying
654 carbon at the sites studied: at DYFAMED, organic carbon fluxes are decorrelated from
655 phytoplankton fluxes. While the maximum biological fluxes to the trap are in the spring, the
656 organic carbon flux is maximum in the summer. At this site, the diatom peak is delayed relative
657 to the peak fluxes in coccoliths, suggesting that diatoms could be responsible for more carbon
658 burial in the sediments.

659 Previous studies have shown that carbon export from the surface increases when diatoms
660 dominate, while smaller phytoplankton, such as coccolithophores, are thought to contribute
661 less to carbon export towards the deep sea because of their slower sinking rates and recycling
662 in the microbial loop (Jin et al., 2006). This principle has been refined, with small nanoplankton
663 blooms now acknowledged for their role in carbon burial (Leblanc et al., 2018; Richardson &
664 Jackson, 2007), in particular as phytoplankton aggregates can counterbalance this effect by
665 increasing the sinking rate of the particles. Nevertheless, our results suggest it remains
666 applicable in the NW Mediterranean Sea: plotting the particle flux against the organic carbon
667 flux shows that in recent years in the Gulf of Lion, a smaller biological particle input to the
668 sediment trap buries more carbon than at the beginning of the studied period (**Figure 10**). Such
669 a trend is not evident in the Ligurian Sea, where instead carbon burial becomes less sensitive to
670 the phytoplankton flux to the trap between 2012 and 2017. The larger input of organic carbon
671 to the sediment per particle to the sea floor in the Gulf of Lion can be related to the increasing
672 occurrence of opal-bearing species in the assemblage (**Figure 11**).

673

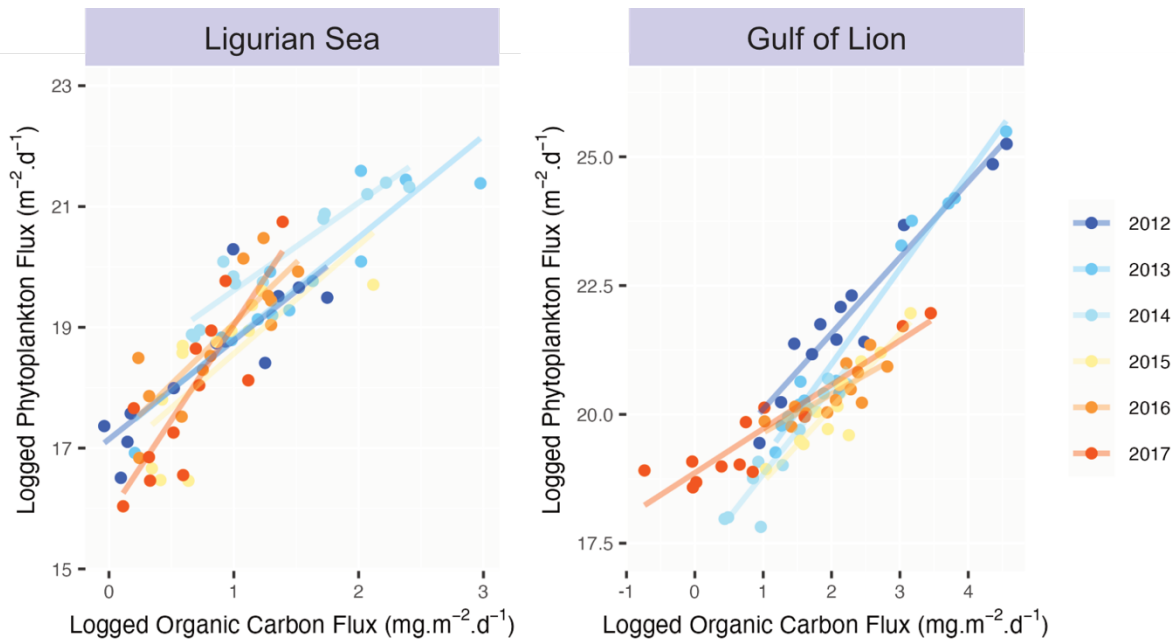


Figure 10 – Evolution of POC burial across the period of study. Points and best fit are colored by year. Maximum POC and phytoplankton fluxes decrease at both sites over the period 2012-2017. However, in the Ligurian Sea, organic carbon burial is decreasing faster than the biological fluxes to the trap (*i.e.* the slope is increasing), suggesting decreasing carbon burial efficiency, while the Ligurian Sea displays the opposite trend. We link these trends to the opposing trends in phytoplankton size structure observed at the sites.

674

675 5 Conclusions

676 In this study we explored the biological record of two sediment trap series in the Northwestern
 677 Mediterranean Sea: the Ligurian Sea and the Gulf of Lion. Our findings document the seasonal
 678 and interannual variations in both the fluxes of biological particles collected in the sediment
 679 traps, and in the composition of the assemblage. The export of biological particles to the traps
 680 appears to be decreasing in both locations. Indeed, the biological fluxes to the sea floor are
 681 adversely affected by a reduction in vertical mixing, which reduces the nutrient input to the
 682 surface – a trend increasingly observed in the NW Mediterranean Sea. In the Gulf of Lion, halts
 683 in the deep convection episodes that occur regularly in the winter lead to a significant
 684 reduction in particle fluxes, which likely reflects both the absence of resuspension episodes and
 685 decreased ventilation and nutrient input to the surface. At both sites, there is a shift toward
 686 assemblages dominated by the biological particles most associated with summer and autumn
 687 conditions, correlating most with the increasing temperatures at the site. However, while the
 688 Ligurian Sea record is increasingly dominated by small coccoliths produced by deep-dwelling
 689 species, the Gulf of Lion displays a shift towards opal-bearing species, including large centric
 690 diatoms and silicoflagellates. These differences likely result from site-specific environmental
 691 trends, including nutrient inputs and pH, although more comprehensive environmental data are
 692 needed to identify the drivers. Finally, we show that these trends in relative assemblages lead

693 to contrasted evolutions of the phytoplankton size structure between the two sites, with
694 consequences on the carbon export at depth. Specifically, we show that a transition towards
695 large and robust siliceous species in the Gulf of Lion increases the burial efficiency of carbon at
696 depth, whereas in the Ligurian Sea, the shift toward smaller phytoplankton reduces it. These
697 findings highlight the complex relationship between environmental changes and biological
698 responses, offering new insights into how climate-driven ocean changes influence carbon
699 cycling in the Mediterranean.

700

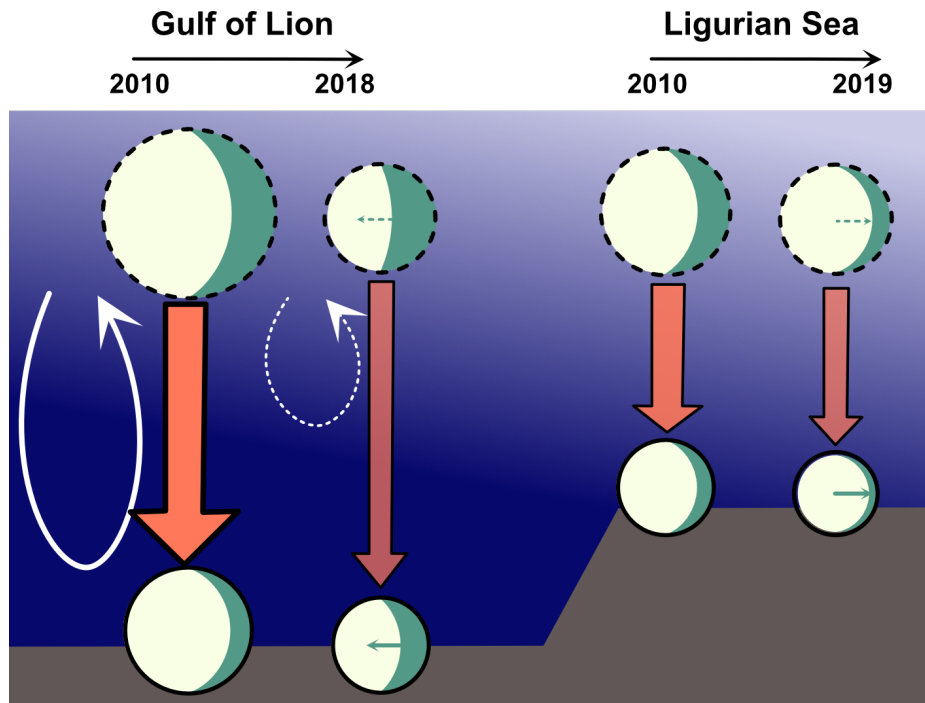


Figure 11 – Schematic representation of carbon burial evolutions in the NW Mediterranean Sea between 2010 and 2019. POC concentrations are shown in the circles, with POC originating from siliceous material, including diatoms, in green, and from coccolithophores in yellow. The orange arrows represent the particle fluxes. Convection dynamics are shown with the white arrow. The POC content in the surface layer was not constrained in this study, and thus is essentially hypothesized. Diatoms are probably relatively more present in the surface POC than at depth, being more exposed to fragmentation and/or dissolution in the water column. At the beginning of the interval, the diatom/coccosphere ratio in the particle flux to the sediment trap is about the same at both sites. Deep convection episodes enhance particle fluxes and POC burial, either through enhanced biological activity in the surface, or faster transport through the water column. They boost primary production in the Ligurian Sea as well. At the end of the interval: the interruption of deep-convection episodes decreases POC production at both sites, and leads to a decrease in particle fluxes to the sea floor. The relative increase of large siliceous particles in the total assemblage at depth in the Gulf of Lion probably reflects, in part, enhanced diatom production in the surface, as some siliceous taxa show increasing flux trends over the study period (e.g. *Bacteriastrum* sp., *Navicula*-like). Coccolithophores might also be decreasing at the site due to higher acidification trends than in the Ligurian Sea. The particle fluxes at Lionceau towards the end of the interval are around the same than at DYFAMED, but siliceous particles are more efficient at exporting POC, therefore POC burial remains higher in the Lionceau sediment trap than at DYFAMED.

701

702 **Acknowledgments**

703 We would like to thank Nathalie Leblond and Laurent Coppola for access to the DYFAMED
704 sediment trap samples. We would like to thank Jean-Charles Mazur and Sandrine Conrod for
705 help with the sample preparation, the OSU Pythéas SIP team for the server support, and Ross
706 Marchant and Thang D. Q. Le for the IT support during the project. We acknowledge the EMSO
707 European Research Infrastructure Consortium and the OceanSITES program, of which the
708 DYFAMED and LION moorings are a part of. This work received support from the French
709 government under the France 2030 investment plan, as part of the Initiative d'Excellence d'Aix-
710 Marseille Université – A*MIDEX (AMX-19-IET-012). The authors declare no conflict of interest.

711

712 **Data Availability Statement:** Data for phytoplankton counts, fluxes, and sizes will be made
713 available on SEANOE upon acceptance of the manuscript.

714

715 **References**

- 716 Abrantes, F. (1999). Water column and recent sediment data on diatoms and coccolithophorids,
717 off Portugal, confirm sediment record of upwelling events. *Oceanologica Acta*, 22(3),
718 319–336. [https://doi.org/10.1016/S0399-1784\(99\)80055-3](https://doi.org/10.1016/S0399-1784(99)80055-3)
- 719 Beaufort, L., Bolton, C. T., Sarr, A.-C., Suchéras-Marx, B., Rosenthal, Y., Donnadieu, Y., Barbarin,
720 N., Bova, S., Cornuault, P., Gally, Y., Gray, E., Mazur, J.-C., & Tetard, M. (2022). Cyclic
721 evolution of phytoplankton forced by changes in tropical seasonality. *Nature*, 601(7891),
722 79–84. <https://doi.org/10.1038/s41586-021-04195-7>
- 723 Beaufort, L., & Dollfus, D. (2004). Automatic recognition of coccoliths by dynamical neural
724 networks. *Marine Micropaleontology*, 51(1–2), 57–73.
725 <https://doi.org/10.1016/j.marmicro.2003.09.003>
- 726 Beaufort, L., Gally, Y., Suchéras-marx, B., Ferrand, P., & Duboisset, J. (2020). *Technical Note: A*
727 *universal method for measuring the thickness of microscopic calcite crystals, based on*
728 *Bidirectional Circular Polarization*. <https://doi.org/10.5194/bg-2020-28>
- 729 Beaufort, L., & Heussner, S. (2001). Seasonal dynamics of calcareous nannoplankton on a West
730 European continental margin: The Bay of Biscay. *Marine Micropaleontology*, 43(1–2),
731 27–55. [https://doi.org/10.1016/S0377-8398\(01\)00020-2](https://doi.org/10.1016/S0377-8398(01)00020-2)
- 732 Beaugrand, G. (2004). The North Sea regime shift: Evidence, causes, mechanisms and
733 consequences. *Progress in Oceanography*, 60(2–4), 245–262.
734 <https://doi.org/10.1016/j.pocean.2004.02.018>
- 735 Bethoux, J. P., & Gentili, B. (1999). Functioning of the Mediterranean Sea: Past and present
736 changes related to freshwater input and climate changes. *Journal of Marine Systems*,
737 20(1–4), 33–47. [https://doi.org/10.1016/S0924-7963\(98\)00069-4](https://doi.org/10.1016/S0924-7963(98)00069-4)

738 Bosse, A., Testor, P., Coppola, L., Bretel, P., Dausse, D., Durrieu De Madron, X., Houpert, L.,
739 Labaste, M., Legoff, H., Mortier, L., & D'ortenzio, F. (2023). *LION observatory data*
740 [Dataset]. SEANOE. <https://doi.org/10.17882/44411>

741 Bosse, A., Testor, P., Mayot, N., Prieur, L., D'Ortenzio, F., Mortier, L., Le Goff, H., Gourcuff, C.,
742 Coppola, L., Lavigne, H., & Raimbault, P. (2017). A submesoscale coherent vortex in the L
743 igurian Sea: From dynamical barriers to biological implications. *Journal of Geophysical*
744 *Research: Oceans*, 122(8), 6196–6217. <https://doi.org/10.1002/2016JC012634>

745 Bown, P. R., Dunkley Jones, T., Young, J. R., & Randell, R. (2009). A PALAEOGENE RECORD OF
746 EXTANT LOWER PHOTIC ZONE CALCAREOUS NANNOPLANKTON. *Palaeontology*, 52(2),
747 457–469. <https://doi.org/10.1111/j.1475-4983.2009.00853.x>

748 Brun, P., Vogt, M., Payne, M. R., Gruber, N., O'Brien, C. J., Buitenhuis, E. T., Le Quéré, C.,
749 Leblanc, K., & Luo, Y. (2015). Ecological niches of open ocean phytoplankton taxa.
750 *Limnology and Oceanography*, 60(3), 1020–1038. <https://doi.org/10.1002/lno.10074>

751 Buesseler, K. O., Antia, A. N., Chen, M., Fowler, S. W., Gardner, W. D., Gustafsson, O., Harada,
752 K., Michaels, A. F., Rutgers Van Der Loeff, M., Sarin, M., Steinberg, D. K., & Trull, T.
753 (2007). An assessment of the use of sediment traps for estimating upper ocean particle
754 fluxes. *Journal of Marine Research*, 65(3), 345–416.
755 <https://doi.org/10.1357/002224007781567621>

756 Canals, M., Puig, P., de Madron, X. D., Heussner, S., Palanques, A., & Fabres, J. (2006). Flushing
757 submarine canyons. *Nature*, 444(7117), 354–357. <https://doi.org/10.1038/nature05271>

758 Ciancia, E., Lacava, T., Pergola, N., Vellucci, V., Antoine, D., Satriano, V., & Tramutoli, V. (2021).
759 Quantifying the Variability of Phytoplankton Blooms in the NW Mediterranean Sea with
760 the Robust Satellite Techniques (RST). *Remote Sensing*, 13(24), 5151.
761 <https://doi.org/10.3390/rs13245151>

762 Conan, P., Testor, P., Estournel, C., D'Ortenzio, F., Pujo-Pay, M., & Durrieu De Madron, X.
763 (2018). Preface to the Special Section: Dense Water Formations in the Northwestern
764 Mediterranean: From the Physical Forcings to the Biogeochemical Consequences.
765 *Journal of Geophysical Research: Oceans*, 123(10), 6983–6995.
766 <https://doi.org/10.1029/2018JC014301>

767 Coppola, L. (2016). *MOOSE-GE 2016 cruise, L'Atalante R/V*. Sismar.
768 <https://doi.org/10.17600/16000700>

769 Coppola, L., Diamond Riquier, E., Carval, T., Irisson, J.-O., & Desnos, C. (2024). *Dyfamed*
770 *observatory data*. [Dataset]. SEANOE. <https://doi.org/10.17882/43749>

771 Coppola, L., & Durrieu De Madron, X. (2020). *MOOSE-GE 2020 cruise, Téthys II R/V*. Sismar.
772 <https://doi.org/10.17600/18000560>

773 Coppola, L., & Testor, P. (2019). *MOOSE-GE 2019 cruise, Thalassa R/V*. Sismar.
774 <https://doi.org/10.17600/18000562>

775 Cramer, W., Guiot, J., Fader, M., Garrabou, J., Gattuso, J.-P., Iglesias, A., Lange, M. A., Lionello,
776 P., Llasat, M. C., Paz, S., Peñuelas, J., Snoussi, M., Toreti, A., Tsimplis, M. N., & Xoplaki, E.

777 (2018). Climate change and interconnected risks to sustainable development in the
778 Mediterranean. *Nature Climate Change*, 8(11), 972–980.
779 <https://doi.org/10.1038/s41558-018-0299-2>

780 Di Pane, J., Wiltshire, K. H., McLean, M., Boersma, M., & Meunier, C. L. (2022). Environmentally
781 induced functional shifts in phytoplankton and their potential consequences for
782 ecosystem functioning. *Global Change Biology*, 28(8), 2804–2819.
783 <https://doi.org/10.1111/gcb.16098>

784 D’Ortenzio, F. (2009). *On the trophic regimes of the Mediterranean Sea: A satellite analysis*.

785 Durrieu De Madron, X., Houpert, L., Puig, P., Sanchez-Vidal, A., Testor, P., Bosse, A., Estournel,
786 C., Somot, S., Bourrin, F., Bouin, M. N., Beauverger, M., Beguery, L., Calafat, A., Canals,
787 M., Cassou, C., Coppola, L., Dause, D., D’Ortenzio, F., Font, J., ... Raimbault, P. (2013).
788 Interaction of dense shelf water cascading and open-sea convection in the northwestern
789 Mediterranean during winter 2012. *Geophysical Research Letters*, 40(7), 1379–1385.
790 <https://doi.org/10.1002/grl.50331>

791 Durrieu de Madron, X., Ramondenc, S., Berline, L., Houpert, L., Bosse, A., Martini, S., Guidi, L.,
792 Conan, P., Curtil, C., Delsaut, N., Kunesch, S., Ghiglione, J. F., Marsaleix, P., Pujo-Pay, M.,
793 Séverin, T., Testor, P., & Tamburini, C. (2017). Deep sediment resuspension and thick
794 nepheloid layer generation by open-ocean convection. *Journal of Geophysical Research:
795 Oceans*, 122(3), 2291–2318. <https://doi.org/10.1002/2016JC012062>

796 Falkowski, P. G., & Oliver, M. J. (2007). Mix and match: How climate selects phytoplankton.
797 *Nature Reviews Microbiology*, 5(10), 813–819. <https://doi.org/10.1038/nrmicro1751>

798 Finkel, Z. V., Beardall, J., Flynn, K. J., Quigg, A., Rees, T. A. V., & Raven, J. A. (2010).
799 Phytoplankton in a changing world: Cell size and elemental stoichiometry. *Journal of
800 Plankton Research*, 32(1), 119–137. <https://doi.org/10.1093/plankt/fbp098>

801 Fourrier, M., Coppola, L., D’Ortenzio, F., Migon, C., & Gattuso, J. (2022). Impact of Intermittent
802 Convection in the Northwestern Mediterranean Sea on Oxygen Content, Nutrients, and
803 the Carbonate System. *Journal of Geophysical Research: Oceans*, 127(9), 1–18.
804 <https://doi.org/10.1029/2022jc018615>

805 Garcia, T., Bănar, D., Guilloux, L., Cornet, V., Gregori, G., & Carlotti, F. (2023). Temporal
806 changes in zooplankton indicators highlight a bottom-up process in the Bay of Marseille
807 (NW Mediterranean Sea). *PLOS ONE*, 18(10), e0292536.
808 <https://doi.org/10.1371/journal.pone.0292536>

809 Godbillot, C., Marchant, R., Beaufort, L., Leblanc, K., Gally, Y., Le, T. D. Q., Chevalier, C., & De
810 Garidel-Thoron, T. (2024). A New Method for the Detection of Siliceous Microfossils on
811 Sediment Microscope Slides Using Convolutional Neural Networks. *Journal of
812 Geophysical Research: Biogeosciences*, 129(9), e2024JG008047.
813 <https://doi.org/10.1029/2024JG008047>

814 Gogou, A., Sanchez-Vidal, A., Durrieu De Madron, X., Stavrakakis, S., Calafat, A. M., Stabholz,
815 M., Psarra, S., Canals, M., Heussner, S., Stavrakaki, I., & Papathanassiou, E. (2014).

816 Carbon flux to the deep in three open sites of the Southern European Seas (SES). *Journal*
817 *of Marine Systems*, 129, 224–233. <https://doi.org/10.1016/j.jmarsys.2013.05.013>

818 Hafen, R. (2016). *Package stlplus* (Version 0.5.1) [Computer software].
819 <https://github.com/hafen/stlplus>

820 Hassenkam, T., Johnsson, A., Bechgaard, K., & Stipp, S. L. S. (2011). Tracking single coccolith
821 dissolution with picogram resolution and implications for CO₂ sequestration and ocean
822 acidification. *Proceedings of the National Academy of Sciences of the United States of*
823 *America*, 108(21), 8571–8576. <https://doi.org/10.1073/pnas.1009447108>

824 Heimbürger, L.-E., Lavigne, H., Migon, C., D’Ortenzio, F., Estournel, C., Coppola, L., & Miquel, J.-
825 C. (2013). Temporal variability of vertical export flux at the DYFAMED time-series station
826 (Northwestern Mediterranean Sea). *Progress in Oceanography*, 119, 59–67.
827 <https://doi.org/10.1016/j.pocean.2013.08.005>

828 Hernández-Almeida, I., Ausín, B., Saavedra-Pellitero, M., Baumann, K.-H., & Stoll, H. M. (2019).
829 Quantitative reconstruction of primary productivity in low latitudes during the last
830 glacial maximum and the mid-to-late Holocene from a global Florisphaera profunda
831 calibration dataset. *Quaternary Science Reviews*, 205, 166–181.
832 <https://doi.org/10.1016/j.quascirev.2018.12.016>

833 Houpert, L., Durrieu de Madron, X., Testor, P., Bosse, A., D’Ortenzio, F., Bouin, M. N., Dausse,
834 D., Le Goff, H., Kunesch, S., Labaste, M., Coppola, L., Mortier, L., & Raimbault, P. (2016).
835 Observations of open-ocean deep convection in the northwestern Mediterranean Sea:
836 Seasonal and interannual variability of mixing and deep water masses for the 2007-2013
837 Period. *Journal of Geophysical Research: Oceans*, 121(11), 8139–8171.
838 <https://doi.org/10.1002/2016JC011857>

839 Iriarte, J., & González, H. (2004). Phytoplankton size structure during and after the 1997/98 El
840 Niño in a coastal upwelling area of the northern Humboldt Current System. *Marine*
841 *Ecology Progress Series*, 269, 83–90. <https://doi.org/10.3354/meps269083>

842 Jin, X., Gruber, N., Dunne, J. P., Sarmiento, J. L., & Armstrong, R. A. (2006). Diagnosing the
843 contribution of phytoplankton functional groups to the production and export of
844 particulate organic carbon, CaCO₃, and opal from global nutrient and alkalinity
845 distributions. *Global Biogeochemical Cycles*, 20(2), 2005GB002532.
846 <https://doi.org/10.1029/2005GB002532>

847 Josey, S. A., & Schroeder, K. (2023). Declining winter heat loss threatens continuing ocean
848 convection at a Mediterranean dense water formation site. *Environmental Research*
849 *Letters*, 18(2), 024005. <https://doi.org/10.1088/1748-9326/aca9e4>

850 Kessouri, F., Ulses, C., Estournel, C., Marsaleix, P., D’Ortenzio, F., Severin, T., Taillandier, V., &
851 Conan, P. (2018). Vertical Mixing Effects on Phytoplankton Dynamics and Organic
852 Carbon Export in the Western Mediterranean Sea. *Journal of Geophysical Research:*
853 *Oceans*, 123(3), 1647–1669. <https://doi.org/10.1002/2016JC012669>

854 Keuter, S., Silverman, J., Krom, M. D., Sisma-Ventura, G., Yu, J., Tsemel, A., Ben-Ezra, T., Sher, D.,
855 Reich, T., Koplovitz, G., & Frada, M. J. (2022). Seasonal patterns of coccolithophores in

- 856 the ultra-oligotrophic South-East Levantine Basin, Eastern Mediterranean Sea. *Marine*
857 *Micropaleontology*, 175, 102153. <https://doi.org/10.1016/j.marmicro.2022.102153>
- 858 Leblanc, K., Quéguiner, B., Diaz, F., Cornet, V., Michel-Rodriguez, M., Durrieu de Madron, X.,
859 Bowler, C., Malviya, S., Thyssen, M., Grégori, G., Rembauville, M., Grosso, O., Poulain, J.,
860 de Vargas, C., Pujo-Pay, M., & Conan, P. (2018). Nanoplanktonic diatoms are globally
861 overlooked but play a role in spring blooms and carbon export. *Nature Communications*,
862 9(1), 953. <https://doi.org/10.1038/s41467-018-03376-9>
- 863 Li, G., Cheng, L., Zhu, J., Trenberth, K. E., Mann, M. E., & Abraham, J. P. (2020). Increasing ocean
864 stratification over the past half-century. *Nature Climate Change*, 10(12), 1116–1123.
865 <https://doi.org/10.1038/s41558-020-00918-2>
- 866 Lionello, P., & Scarascia, L. (2018). The relation between climate change in the Mediterranean
867 region and global warming. *Regional Environmental Change*, 18(5), 1481–1493.
868 <https://doi.org/10.1007/s10113-018-1290-1>
- 869 Macias, D., Garcia-Gorrioz, E., & Stips, A. (2018). Deep winter convection and phytoplankton
870 dynamics in the NW Mediterranean Sea under present climate and future (horizon
871 2030) scenarios. *Scientific Reports*, 8(1), 6626. [https://doi.org/10.1038/s41598-018-](https://doi.org/10.1038/s41598-018-24965-0)
872 24965-0
- 873 Marchant, R., Tetard, M., Pratiwi, A., Adebayo, M., & De Garidel-Thoron, T. (2020). Automated
874 analysis of foraminifera fossil records by image classification using a convolutional
875 neural network. *Journal of Micropalaeontology*, 39(2), 183–202.
876 <https://doi.org/10.5194/jm-39-183-2020>
- 877 Margalef, R. (1978). Life-forms of phytoplankton as survival alternatives in an unstable
878 environment. *Oceanologica Acta*, 1(4), 493–509.
- 879 Margirier, F., Testor, P., Heslop, E., Mallil, K., Bosse, A., Houpert, L., Mortier, L., Bouin, M.-N.,
880 Coppola, L., D’Ortenzio, F., Durrieu de Madron, X., Mourre, B., Prieur, L., Raimbault, P.,
881 & Taillandier, V. (2020). Abrupt warming and salinification of intermediate waters
882 interplays with decline of deep convection in the Northwestern Mediterranean Sea.
883 *Scientific Reports*, 10(1), 20923. <https://doi.org/10.1038/s41598-020-77859-5>
- 884 Marty, J.-C., Chiavérini, J., Pizay, M.-D., & Avril, B. (2002). Seasonal and interannual dynamics of
885 nutrients and phytoplankton pigments in the western Mediterranean Sea at the
886 DYFAMED time-series station (1991–1999). *Deep Sea Research Part II: Topical Studies in*
887 *Oceanography*, 49(11), 1965–1985. [https://doi.org/10.1016/S0967-0645\(02\)00022-X](https://doi.org/10.1016/S0967-0645(02)00022-X)
- 888 Mayot, N., D’Ortenzio, F., Uitz, J., Gentili, B., Ras, J., Vellucci, V., Golbol, M., Antoine, D., &
889 Claustre, H. (2017). Influence of the Phytoplankton Community Structure on the Spring
890 and Annual Primary Production in the Northwestern Mediterranean Sea. *Journal of*
891 *Geophysical Research: Oceans*, 122(12), 9918–9936.
892 <https://doi.org/10.1002/2016JC012668>
- 893 Mayot, N., Nival, P., & Levy, M. (2020). Primary Production in the Ligurian Sea. In C. Mignon, P.
894 Nival, & A. Sciandra (Eds.), *The Mediterranean Sea in the Era of Global Change 1* (1st ed.,
895 pp. 139–164). Wiley. <https://doi.org/10.1002/9781119706960.ch6>

- 896 Meyer, J., & Riebesell, U. (2015). Reviews and syntheses: Responses of coccolithophores to
897 ocean acidification: A meta-analysis. *Biogeosciences*, *12*(6), 1671–1682.
898 <https://doi.org/10.5194/bg-12-1671-2015>
- 899 Miquel, J.-C., Martín, J., Gasser, B., Rodriguez-y-Baena, A., Toubal, T., & Fowler, S. W. (2011).
900 Dynamics of particle flux and carbon export in the northwestern Mediterranean Sea: A
901 two decade time-series study at the DYFAMED site. *Progress in Oceanography*, *91*(4),
902 461–481. <https://doi.org/10.1016/j.pocean.2011.07.018>
- 903 Oksanen, J., Simpson, G. L., Blanchet, F. G., Kindt, R., Legendre, P., Minchin, P. R., O'Hara, R. B.,
904 Solymos, P., Stevens, M. H. H., Szoecs, E., Wagner, H., Barbour, M., Bedward, M., Bolker,
905 B., Borcard, D., Carvalho, G., Chirico, M., De Caceres, M., Durand, S., ... Weedon, J.
906 (2001). *vegan: Community Ecology Package* (p. 2.6-8) [Dataset].
907 <https://doi.org/10.32614/CRAN.package.vegan>
- 908 Parras-Berrocal, I. M., Vázquez, R., Cabos, W., Sein, D. V., Álvarez, O., Bruno, M., & Izquierdo, A.
909 (2022). Surface and Intermediate Water Changes Triggering the Future Collapse of Deep
910 Water Formation in the North Western Mediterranean. *Geophysical Research Letters*,
911 *49*(4), e2021GL095404. <https://doi.org/10.1029/2021GL095404>
- 912 Pusceddu, A., Mea, M., Canals, M., Heussner, S., Durrieu De Madron, X., Sanchez-Vidal, A.,
913 Bianchelli, S., Corinaldesi, C., Dell'Anno, A., Thomsen, L., & Danovaro, R. (2013). Major
914 consequences of an intense dense shelf water cascading event on deep-sea benthic
915 trophic conditions and meiofaunal biodiversity. *Biogeosciences*, *10*(4), 2659–2670.
916 <https://doi.org/10.5194/bg-10-2659-2013>
- 917 Rembauville, M., Blain, S., Armand, L., Quéguiner, B., & Salter, I. (2015). Export fluxes in a
918 naturally iron-fertilized area of the Southern Ocean – Part 2: Importance of diatom
919 resting spores and faecal pellets for export. *Biogeosciences*, *12*(11), 3171–3195.
920 <https://doi.org/10.5194/bg-12-3171-2015>
- 921 Riaux-Gobin, C. (1996). *Ditylum brightwellii* (Bacillariophyceae): Resting spores at the surface of
922 a shallow sediment (Gulf of Lions, Mediterranean) and revival tests. *Phycologia*, *35*(4),
923 368–371. <https://doi.org/10.2216/i0031-8884-35-4-368.1>
- 924 Richardson, T. L., & Jackson, G. A. (2007). Small Phytoplankton and Carbon Export from the
925 Surface Ocean. *Science*, *315*(5813), 838–840. <https://doi.org/10.1126/science.1133471>
- 926 Riebesell, U., Bach, L. T., Bellerby, R. G. J., Monsalve, J. R. B., Boxhammer, T., Czerny, J., Larsen,
927 A., Ludwig, A., & Schulz, K. G. (2017). Competitive fitness of a predominant pelagic
928 calcifier impaired by ocean acidification. *Nature Geoscience*, *10*(1), 19–23.
929 <https://doi.org/10.1038/ngeo2854>
- 930 Rigual-Hernández, A. S., Bárcena, M. A., Jordan, R. W., Sierro, F. J., Flores, J. A., Meier, K. J. S.,
931 Beaufort, L., & Heussner, S. (2013). Diatom fluxes in the NW Mediterranean: Evidence
932 from a 12-year sediment trap record and surficial sediments. *Journal of Plankton*
933 *Research*, *35*(5), 1109–1125. <https://doi.org/10.1093/plankt/fbt055>
- 934 Rigual-Hernández, A. S., Bárcena, M. A., Sierro, F. J., Flores, J. A., Hernández-Almeida, I.,
935 Sanchez-Vidal, A., Palanques, A., & Heussner, S. (2010). Seasonal to interannual

936 variability and geographic distribution of the silicoflagellate fluxes in the Western
937 Mediterranean. *Marine Micropaleontology*, 77(1–2), 46–57.
938 <https://doi.org/10.1016/j.marmicro.2010.07.003>

939 Ryneerson, T. A., Richardson, K., Lampitt, R. S., Sieracki, M. E., Poulton, A. J., Lyngsgaard, M. M.,
940 & Perry, M. J. (2013). Major contribution of diatom resting spores to vertical flux in the
941 sub-polar North Atlantic. *Deep Sea Research Part I: Oceanographic Research Papers*, 82,
942 60–71. <https://doi.org/10.1016/j.dsr.2013.07.013>

943 Severin, T., Conan, P., Durrieu De Madron, X., Houpert, L., Oliver, M. J., Oriol, L., Caparros, J.,
944 Ghiglione, J. F., & Pujo-Pay, M. (2014). Impact of open-ocean convection on nutrients,
945 phytoplankton biomass and activity. *Deep Sea Research Part I: Oceanographic Research*
946 *Papers*, 94, 62–71. <https://doi.org/10.1016/j.dsr.2014.07.015>

947 Severin, T., Kessouri, F., Rembauville, M., Sánchez-Pérez, E. D., Oriol, L., Caparros, J., Pujo-Pay,
948 M., Ghiglione, J., D’Ortenzio, F., Taillandier, V., Mayot, N., Durrieu De Madron, X., Ulses,
949 C., Estournel, C., & Conan, P. (2017). Open-ocean convection process: A driver of the
950 winter nutrient supply and the spring phytoplankton distribution in the Northwestern
951 Mediterranean Sea. *Journal of Geophysical Research: Oceans*, 122(6), 4587–4601.
952 <https://doi.org/10.1002/2016JC012664>

953 Somot, S., Sevault, F., & Déqué, M. (2006). Transient climate change scenario simulation of the
954 Mediterranean Sea for the twenty-first century using a high-resolution ocean circulation
955 model. *Climate Dynamics*, 27(7–8), 851–879. <https://doi.org/10.1007/s00382-006-0167->
956 [z](https://doi.org/10.1007/s00382-006-0167-z)

957 Sprengel, C., Baumann, K.-H., & Neuer, S. (2000). Seasonal and interannual variation of
958 coccolithophore fluxes and species composition in sediment traps north of Gran Canaria
959 (29°N 15°W). *Marine Micropaleontology*, 39(1–4), 157–178.
960 [https://doi.org/10.1016/S0377-8398\(00\)00019-0](https://doi.org/10.1016/S0377-8398(00)00019-0)

961 Stabholz, M., Durrieu De Madron, X., Canals, M., Khripounoff, A., Taupier-Letage, I., Testor, P.,
962 Heussner, S., Kerhervé, P., Delsaut, N., Houpert, L., Lastras, G., & Dennielou, B. (2013).
963 Impact of open-ocean convection on particle fluxes and sediment dynamics in the deep
964 margin of the Gulf of Lions. *Biogeosciences*, 10(2), 1097–1116.
965 <https://doi.org/10.5194/bg-10-1097-2013>

966 Suikkanen, S., Pulina, S., Engström-Öst, J., Lehtiniemi, M., Lehtinen, S., & Brutemark, A. (2013).
967 Climate Change and Eutrophication Induced Shifts in Northern Summer Plankton
968 Communities. *PLoS ONE*, 8(6), e66475. <https://doi.org/10.1371/journal.pone.0066475>

969 Testor, P. (2017). *MOOSE-GE 2017 cruise, L’Atalante R/V*. Sismar.
970 <https://doi.org/10.17600/17001500>

971 Testor, P., & Coppola, L. (2018). *MOOSE-GE 2018 cruise, L’Atalante R/V*. Sismar.
972 <https://doi.org/10.17600/18000442>

973 Testor, P., Laurent, C., & MORTIER Laurent. (2010). *MOOSE-GE 2010 cruise, Téthys II R/V*.
974 Sismar. <https://doi.org/10.17600/10450080>

- 975 Testor, P., Laurent, C., & MORTIER Laurent. (2011). *MOOSE-GE 2011 cruise, Téthys II R/V*.
976 Sismar. <https://doi.org/10.17600/11450160>
- 977 Testor, P., Laurent, C., & MORTIER Laurent. (2012). *MOOSE-GE 2012 cruise, Le Suroît R/V*.
978 Sismar. <https://doi.org/10.17600/12020030>
- 979 Testor, P., Laurent, C., & MORTIER Laurent. (2013). *MOOSE-GE 2013 cruise, Téthys II R/V*.
980 Sismar. <https://doi.org/10.17600/13450110>
- 981 Testor, P., Laurent, C., & MORTIER Laurent. (2014). *MOOSE-GE 2014 cruise, Le Suroît R/V*.
982 Sismar. <https://doi.org/10.17600/14002300>
- 983 Testor, P., Laurent, C., & MORTIER Laurent. (2015). *MOOSE-GE 2015 cruise, Le Suroît R/V*.
984 Sismar. <https://doi.org/10.17600/15002500>
- 985 Tetard, M., Marchant, R., Cortese, G., Gally, Y., de Garidel-Thoron, T., & Beaufort, L. (2020).
986 Technical note: A new automated radiolarian image acquisition, stacking, processing,
987 segmentation and identification workflow. *Climate of the Past*, 16(6), 2415–2429.
988 <https://doi.org/10.5194/cp-16-2415-2020>
- 989 Thornton, D. C. O. (2002). Diatom aggregation in the sea: Mechanisms and ecological
990 implications. *European Journal of Phycology*, 37(2), 149–161.
991 <https://doi.org/10.1017/S0967026202003657>
- 992 Touratier, F., Goyet, C., Houpert, L., De Madron, X. D., Lefèvre, D., Stabholz, M., & Guglielmi, V.
993 (2016). Role of deep convection on anthropogenic CO₂ sequestration in the Gulf of Lions
994 (northwestern Mediterranean Sea). *Deep Sea Research Part I: Oceanographic Research*
995 *Papers*, 113, 33–48. <https://doi.org/10.1016/j.dsr.2016.04.003>
- 996 Tsiaras, K., Frangoulis, C., & Stamatakis, N. (2024). Carbonate system variability in the
997 Mediterranean Sea: A modelling study. *Frontiers in Marine Science*, 11, 1347990.
998 <https://doi.org/10.3389/fmars.2024.1347990>
- 999 Tyrrell, T., & Merico, A. (2004). *Emiliania huxleyi*: Bloom observations and the conditions that
1000 induce them Introduction: Distribution and environmental effects. *Coccolithophores:*
1001 *From Molecular Processes to Global Impact*, 75–97.
- 1002 Vink, A. (2004). Calcareous dinoflagellate cysts in South and equatorial Atlantic surface
1003 sediments: Diversity, distribution, ecology and potential for palaeoenvironmental
1004 reconstruction. *Marine Micropaleontology*, 50(1–2), 43–88.
1005 [https://doi.org/10.1016/S0377-8398\(03\)00067-7](https://doi.org/10.1016/S0377-8398(03)00067-7)
- 1006 Williams, J. R., Giering, S. L. C., Baker, C. A., Pabortsava, K., Briggs, N., East, H., Espinola, B.,
1007 Blackbird, S., Le Moigne, F. A. C., Villa-Alfageme, M., Poulton, A. J., Carvalho, F., Pebody,
1008 C., Saw, K., Moore, C. M., Henson, S. A., Sanders, R., & Martin, A. P. (2024). Inefficient
1009 transfer of diatoms through the subpolar Southern Ocean twilight zone. *Nature*
1010 *Geoscience*. <https://doi.org/10.1038/s41561-024-01602-2>
- 1011 Yoder, J. A., & Ishimaru, T. (1989). Phytoplankton advection off the southeastern United States
1012 continental shelf. *Continental Shelf Research*, 9(6), 547–553.
1013 [https://doi.org/10.1016/0278-4343\(89\)90020-4](https://doi.org/10.1016/0278-4343(89)90020-4)

- 1014 Ziveri, P., Rutten, A., de Lange, G. J., Thomson, J., & Corselli, C. (2000). Present-day coccolith
1015 fluxes recorded in central eastern Mediterranean sediment traps and surface sediments.
1016 *Palaeogeography, Palaeoclimatology, Palaeoecology*, 158(3–4), 175–195.
1017 [https://doi.org/10.1016/S0031-0182\(00\)00049-3](https://doi.org/10.1016/S0031-0182(00)00049-3)
- 1018 Zúñiga, D., Sanchez-Vidal, A., Flexas, M. M., Carroll, D., Rufino, M. M., Spreen, G., Calafat, A., &
1019 Abrantes, F. (2021). Sinking Diatom Assemblages as a Key Driver for Deep Carbon and
1020 Silicon Export in the Scotia Sea (Southern Ocean). *Frontiers in Earth Science*, 9, 579198.
1021 <https://doi.org/10.3389/feart.2021.579198>
- 1022